

Efficient optomechanical refrigeration of two vibrations via an auxiliary feedback loop: Giant enhancement in mechanical susceptibilities and net cooling rates


Deng-Gao Lai,^{1,*} Wei Qin^{1,†}, Adam Miranowicz^{1,2,‡} and Franco Nori^{1,3,4,§}

¹Theoretical Quantum Physics Laboratory, RIKEN Cluster for Pioneering Research, Wako-shi, Saitama 351-0198, Japan

²Institute of Spintronics and Quantum Information, Faculty of Physics, Adam Mickiewicz University, 61-614 Poznań, Poland

³RIKEN Center for Quantum Computing (RQC), 2-1 Hirosawa, Wako-shi, Saitama 351-0198, Japan

⁴Physics Department, University of Michigan, Ann Arbor, Michigan 48109-1040, USA

 (Received 23 December 2021; revised 30 April 2022; accepted 9 June 2022; published 5 August 2022)

We propose a method to realize the simultaneous ground-state refrigeration of two vibrational modes *beyond* the resolved-sideband regime via an auxiliary feedback loop (AFL). This is realized by introducing the AFL to *break the dark mode*, which is formed by two vibrational modes coupled to a common cavity-field mode. We obtain analytical results of the effective mechanical susceptibilities and net-refrigeration rates, and find that in the presence of the AFL a *giant enhancement* can be achieved for these susceptibilities and refrigeration rates. Remarkably, the net-cooling rates under the AFL mechanism can be up to *four orders of magnitude* larger than those in cases without the AFL. Moreover, we show that the simultaneous ground-state refrigeration arises from the AFL mechanism, without which it vanishes. This is because in the absence of the AFL, the dark mode prevents energy extraction through the cooling channels. However, by introducing the AFL, dark-mode breaking rebuilds the refrigeration channels, and, as a result, leads to the simultaneous cooling of these vibrations. Our approach has remarkable flexibility and scalability and can be extended to the simultaneous refrigeration of a large number of vibrations beyond the resolved-sideband regime.

DOI: [10.1103/PhysRevResearch.4.033102](https://doi.org/10.1103/PhysRevResearch.4.033102)

I. INTRODUCTION

Quantum manipulation of multiple-vibrational-mode systems has become an important research topic in cavity optomechanics [1–3]. These systems not only provide a unique platform to study macroscopic mechanical coherence [4–15], topological energy transfer [16], and quantum many-body phenomena [17–24], but also can be widely applied in quantum mechanical computers [25,26], high-performance sensors [27–29], and nonreciprocal devices [30–37]. To observe significant quantum mechanical effects of multiple-vibration systems, a prerequisite is to simultaneously cool these systems to their quantum ground states by effectively suppressing their thermal noises.

So far, two effective cooling mechanisms using cavity optomechanics have been proposed to cool a single mechanical mode to its quantum ground state, i.e., (i) cavity-resolved sideband cooling [38,39], which is more efficient in the good-cavity regime, and (ii) feedback-aided cooling [40–54], which is preferable in the bad-cavity regime. To

further improve the refrigeration efficiency of a mechanical mode, various new cooling schemes have been proposed, such as those based on strong couplings [55,56], quantum interference effect [57–59], modulated pulses [60,61], nonreciprocity [34,62], and domino effect [63,64]. In particular, the refrigeration of a mechanical resonator has been widely studied in both optical [65–69] and microwave [70–76] domains. Despite such achievements, the simultaneous refrigeration of multiple vibrations remains a major challenge in cavity optomechanics. This is due to cooling suppression originating from dark modes [77,78], which are induced by coupling multiple vibrational modes to a common optical mode [6,49,79–82]. Recently, based on the resolved-sideband-cooling mechanism, a dark-mode-breaking method using an auxiliary-cavity mode has been developed for cooling multiple mechanical resonators in the good-cavity regime [83,84]. However, the answer to the question of whether one can skillfully combine this method and the feedback-cooling technique to simultaneously cool these mechanical resonators in the bad-cavity regime is yet unclear.

Here, based on the feedback-cooling mechanism [40–51], we propose to simultaneously cool two vibrational modes to their quantum ground states by breaking the dark mode via an auxiliary feedback loop (AFL). We obtain the *exact analytical* solutions of effective mechanical susceptibilities, net-cooling rates, and mechanical frequency shifts. Then, we find that when switching the AFL-off to AFL-on cases, the net-refrigeration rates can be increased from γ_m up to $10^4\gamma_m$, where γ_m is a mechanical decay rate. In particular, the net-refrigeration rates under the AFL mechanism can be

*Corresponding author: denggaolai@foxmail.com

†wei.qin@riken.jp

‡miran@amu.edu.pl

§fnori@riken.jp

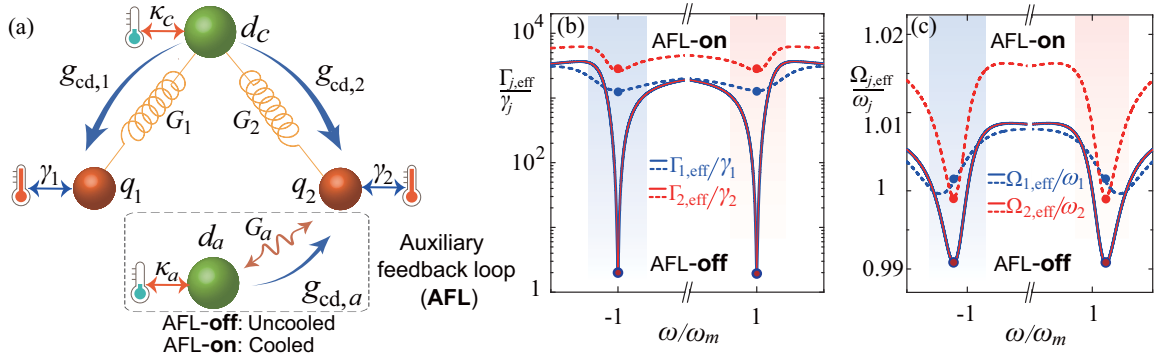


FIG. 1. (a) Schematics of a multimode optomechanical system. Two mechanical modes $q_{j=1,2}$ (both with resonance frequency ω_m and mechanical decay rate γ_j) are coupled to a common cooling-cavity mode d_c (with resonance frequency ω_c and cavity-field decay rate κ_c) via the radiation-pressure couplings of strengths G_j . An auxiliary cavity d_a (with resonance frequency ω_a and cavity-field decay rate κ_a) is coupled to the second mechanical mode via an optomechanical coupling strength G_a . The output fields of the two driven cavities are measured via homodyne detection, and then the feedback loops (with optomechanical couplings $G_{k=1,2,a}$ and feedback gains $g_{cd,k=1,2,a}$) are utilized to design direct forces exerted on the two mechanical modes, which can lead to the freezing of their thermal fluctuations (i.e., the cold-damping effect) [40–51]. (b) Effective mechanical damping $\Gamma_{j,\text{eff}}(\omega)$ [see Eq. (22a)] and (c) effective mechanical frequency $\Omega_{j,\text{eff}}(\omega)$ [see Eqs. (22b) and (22c)] vs the Fourier frequency ω in the AFL-off ($G_a = 0$ and $g_{cd,a} = 0$, solid curves) and AFL-on ($G_a/\omega_m = 0.2$ and $g_{cd,a} = 0.5$, dashed curves) cases. The parameters used here are $\tilde{\Delta}_c = \tilde{\Delta}_a = 0$, $\omega_{j=1,2} = \omega_m$, $\kappa_c = \kappa_a = 3\omega_m$, $\gamma_{j=1,2} = 10^{-5}\omega_m$, $G_{j=1,2} = 0.2\omega_m$, $g_{cd,j=1,2} = 0.5$, $\zeta_c = \zeta_a = 0.8$, and $\omega_{\text{fb},j=1,2} = \omega_{\text{fb},a} = 4\omega_m$.

tremendously amplified by appropriately designing the AFL. These tremendously amplified net-cooling rates lead to a *giant enhancement* in the cooling performance of the vibrational modes.

Remarkably, we find that for the AFL-off case, the simultaneous refrigeration of two vibrational modes fails due to the cooling suppression from the dark mode, while for the AFL-on case, a high efficient ground-state cooling of these vibrations is achieved, beyond the resolved-sideband regime, by breaking the dark mode. Physically, the AFL mechanism provides a useful strategy to break the dark mode and, in turn, to rebuild cooling channels for extracting thermal phonons stored in the dark mode. Moreover, we find that due to the use of the AFL, the cooling efficiency is higher for the mechanical mode connected to the AFL. Our model is generic and can provide a way to simultaneously cool a large number of vibrational modes in the unresolved-sideband regime via dark-mode breaking.

The rest of this paper is organized as follows. In Sec. II, we present a multiple-mode optomechanical model with the AFL and its Hamiltonian. In Sec. III, we derive the Langevin equations, show the cold-damping feedback, obtain the steady-state average phonon numbers, and analyze the dark-mode control. In Sec. IV, we analyze the multiple-mode optomechanical refrigeration via the AFL. In Sec. V, we analyze the optical dark mode, seek optimal feedback parameters, and give some discussions. In Sec. VI, we generalize our method to the loop-coupled system and give possible experimental realizations. Finally, we conclude in Sec. VII. The Appendix includes the detailed parameter expressions of the effective mechanical susceptibilities.

II. MODEL AND HAMILTONIAN

We focus on a multimode optomechanical system, where a cooling-cavity-field mode is optomechanically coupled to two

vibrational modes. To control the dark mode in the system, we introduce an auxiliary-cavity-field mode, which is coupled to the second mechanical mode via a radiation-pressure interaction, as illustrated in Fig. 1(a). For the sake of manipulating the mechanical and optical degrees of freedom, a monochromatic laser, with field amplitude Ω_L (Ω_R) and frequency ω_L (ω_R), is used to drive the cooling (auxiliary) cavity. The output fields of the two driven cavities are measured via homodyne detection, and then the feedback loops are utilized to design direct forces applied upon the two mechanical modes, which can lead to the freezing of their thermal fluctuations (i.e., the cold-damping effect) [40,41,43–51]. In a rotating frame defined by $\exp(-i\omega_L t d_c^\dagger d_c - i\omega_R t d_a^\dagger d_a)$, the Hamiltonian of the system reads ($\hbar = 1$)

$$H_I = \Delta_c d_c^\dagger d_c + \Delta_a d_a^\dagger d_a + \sum_{j=1}^2 \left[\frac{\omega_j (p_j^2 + q_j^2)}{2} - \lambda_j d_c^\dagger d_c q_j \right] - \lambda_a d_a^\dagger d_a q_2 + (\Omega_L d_c^\dagger + \Omega_R d_a^\dagger + \text{H.c.}), \quad (1)$$

where $\Delta_c = \omega_c - \omega_L$ and $\Delta_a = \omega_a - \omega_R$ are, respectively, the driving detunings of the cooling-cavity and auxiliary-cavity fields of resonance frequencies ω_c and ω_a . The operators d_c^\dagger and d_a^\dagger (d_c and d_a) are the creation (annihilation) operators of the cooling-cavity and auxiliary-cavity modes, respectively. The j th mechanical mode is described by the dimensionless momentum (p_j) and coordinate (q_j) operators with resonance frequency ω_j . The λ_j term in Eq. (1) describes the optomechanical interaction between the cooling-cavity field and the j th mechanical mode, where $\lambda_j = \omega_c/L\sqrt{1/(m_j\omega_j)}$ is the strength of a single-photon optomechanical coupling, with L and m_j being the rest length of the cooling cavity and the mass of the j th mechanical mode, respectively. The interaction (with strength λ_a) between the auxiliary cavity and the second mechanical mode is described by the λ_a term. The last term in Eq. (1) describes, respectively, the laser driving

of the cooling and auxiliary cavities, whose amplitudes are $\Omega_L = \sqrt{2P_L\kappa_c}/\omega_L$ and $\Omega_R = \sqrt{2P_R\kappa_a}/\omega_R$, with κ_c (κ_a) and P_L (P_R) denoting the cavity-field decay rate and the driving power for the cooling (auxiliary) cavity, respectively. Our physical model could be implemented using a Fabry-Prot-cavity optomechanical configuration, where a double-movable-mirror optomechanical cavity is coupled to another cavity field, as shown in Sec. VI.

III. LANGEVIN EQUATIONS, DARK-MODE CONTROL, COLD-DAMPING FEEDBACK, AND FINAL MEAN PHONON NUMBERS

In this section, we derive the Langevin equations of the system, analyze cold-damping feedback, and obtain the final steady-state mean phonon numbers of the two mechanical modes.

A. Langevin equations

To include the damping and noise effects, we consider the case where the two cavity-field modes are coupled to their vacuum baths, and the two mechanical modes are subjected to quantum Brownian forces. Then, the evolution of this system can be described by the quantum Langevin equations:

$$\dot{d}_c = -i\Delta_c d_c + \sum_{j=1}^2 i\lambda_j d_c q_j - i\Omega_L - \kappa_c d_c + \sqrt{2\kappa_c} d_{c,\text{in}}, \quad (2a)$$

$$\dot{d}_a = -(i\Delta_a + \kappa_a) d_a + i\lambda_a d_a q_2 - i\Omega_R + \sqrt{2\kappa_a} d_{a,\text{in}}, \quad (2b)$$

$$\dot{p}_1 = -\omega_1 q_1 + \lambda_1 d_c^\dagger d_c - \gamma_1 p_1 + \xi_1, \quad (2c)$$

$$\dot{p}_2 = -\omega_2 q_2 + \lambda_2 d_c^\dagger d_c + \lambda_a d_a^\dagger d_a - \gamma_2 p_2 + \xi_2, \quad (2d)$$

$$\dot{q}_j = \omega_j p_j, \quad (2e)$$

where γ_j denotes the decay rate of the j th vibrational mode. The operators $d_{c,\text{in}}$ ($d_{a,\text{in}}$) and ξ_j are, respectively, the noise operators of the cooling (auxiliary) cavity mode and the Brownian force acting on the j th vibrational mode. These noise operators have zero mean values and satisfy the following correlation functions:

$$\langle d_{c,\text{in}}(t) d_{c,\text{in}}^\dagger(t') \rangle = \delta(t - t'), \quad \langle d_{c,\text{in}}^\dagger(t) d_{c,\text{in}}(t') \rangle = 0, \quad (3a)$$

$$\langle d_{a,\text{in}}(t) d_{a,\text{in}}^\dagger(t') \rangle = \delta(t - t'), \quad \langle d_{a,\text{in}}^\dagger(t) d_{a,\text{in}}(t') \rangle = 0, \quad (3b)$$

$$\begin{aligned} \langle \xi_j(t) \xi_j(t') \rangle &= \frac{\gamma_j}{\omega_j} \int e^{-i\omega(t-t')\omega} \\ &\times \left[\coth\left(\frac{\omega}{2k_B T_j}\right) + 1 \right] \frac{d\omega}{2\pi}, \end{aligned} \quad (3c)$$

where T_j is the thermal-reservoir temperature associated with the j th vibrational mode, and k_B is the Boltzmann constant.

To cool these vibrational modes, we consider the strong-driving regime of the two cavities. In this case, the mean photon number in the two cavities is sufficiently large, and then a linearization procedure can be used to simplify our physical model. To this end, the operators in Eq. (2) can be written as the sums of averages and fluctuations, i.e., $o = \langle o \rangle_{\text{ss}} + \delta o$, for d_c , d_c^\dagger , d_a , d_a^\dagger , q_j , and p_j . We separate the

quantum fluctuations and classical motions, and then write the linearized quantum Langevin equations as

$$\delta\dot{X}_c = -\kappa_c \delta X_c + \tilde{\Delta}_c \delta Y_c + \sqrt{2\kappa_c} X_c^{\text{in}}, \quad (4a)$$

$$\delta\dot{Y}_c = -\tilde{\Delta}_c \delta X_c - \kappa_c \delta Y_c + \sum_{j=1}^2 G_j \delta q_j + \sqrt{2\kappa_c} Y_c^{\text{in}}, \quad (4b)$$

$$\delta\dot{X}_a = -\kappa_a \delta X_a + \tilde{\Delta}_a \delta Y_a + \sqrt{2\kappa_a} X_a^{\text{in}}, \quad (4c)$$

$$\delta\dot{Y}_a = -\tilde{\Delta}_a \delta X_a - \kappa_a \delta Y_a + G_a \delta q_2 + \sqrt{2\kappa_a} Y_a^{\text{in}}, \quad (4d)$$

$$\delta\dot{p}_1 = -\omega_1 \delta q_1 + G_1 \delta X_c - \gamma_1 \delta p_1 + \xi_1, \quad (4e)$$

$$\delta\dot{p}_2 = -\omega_2 \delta q_2 + G_2 \delta X_c + G_a \delta X_a - \gamma_2 \delta p_2 + \xi_2, \quad (4f)$$

$$\delta\dot{q}_j = \omega_j \delta p_j, \quad (4g)$$

where $\delta X_l = (\delta d_l^\dagger + \delta d_l)/\sqrt{2}$ and $\delta Y_l = i(\delta d_l^\dagger - \delta d_l)/\sqrt{2}$ (for $l = c, a$) are the quadratures of the cooling and auxiliary cavity fields, and $X_l^{\text{in}} = (d_{l,\text{in}}^\dagger + d_{l,\text{in}})/\sqrt{2}$ and $Y_l^{\text{in}} = i(d_{l,\text{in}}^\dagger - d_{l,\text{in}})/\sqrt{2}$ denote the corresponding Hermitian input noise quadratures. In addition, we have defined the normalized driving detunings $\tilde{\Delta}_c = \Delta_c - \sum_{j=1}^2 \lambda_j \langle q_j \rangle_{\text{ss}}$ ($\tilde{\Delta}_a = \Delta_a - \lambda_a \langle q_2 \rangle_{\text{ss}}$) and the effective optomechanical couplings $G_j = \sqrt{2} \lambda_j \langle d_c \rangle_{\text{ss}}$ ($G_a = \sqrt{2} \lambda_a \langle d_a \rangle_{\text{ss}}$) with $\langle d_c \rangle_{\text{ss}} = -i\Omega_L/(\kappa_c + i\tilde{\Delta}_c)$ and $\langle d_a \rangle_{\text{ss}} = -i\Omega_R/(\kappa_a + i\tilde{\Delta}_a)$.

B. Cold-damping feedback

For the sake of achieving the *cold-damping feedback*, we consider the case of $\tilde{\Delta}_c = 0$ and $\tilde{\Delta}_a = 0$, corresponding to the *highest sensitivity* for the position measurements of the mechanical modes [40,49]. Note that this is essentially *different from the sideband cooling mechanism*, which requires the red-sideband resonance, i.e., $\tilde{\Delta}_c = \omega_j$ and $\tilde{\Delta}_a = \omega_j$ [38,39]. By using a negative derivative feedback, the effective decay rate of the mechanical mode can be largely developed by the cold-damping feedback technique [40–51].

Physically, the position of the two mechanical modes is measured through the phase-sensitive detection of the cavity output field, and then the readout of the cavity output field is fed back onto the two mechanical modes by applying feedback forces. The intensity of the feedback forces is proportional to the time derivative of the output signal, and, therefore, to the velocity of the mechanical modes [40,41,43–51]. Then, the linearized quantum Langevin equations under the feedback scheme read

$$\delta\dot{X}_c = -\kappa_c \delta X_c + \sqrt{2\kappa_c} X_c^{\text{in}}, \quad (5a)$$

$$\delta\dot{Y}_c = -\kappa_c \delta Y_c + \sum_{j=1}^2 G_j \delta q_j + \sqrt{2\kappa_c} Y_c^{\text{in}}, \quad (5b)$$

$$\delta\dot{X}_a = -\kappa_a \delta X_a + \sqrt{2\kappa_a} X_a^{\text{in}}, \quad (5c)$$

$$\delta\dot{Y}_a = -\kappa_a \delta Y_a + G_a \delta q_2 + \sqrt{2\kappa_a} Y_a^{\text{in}}, \quad (5d)$$

$$\begin{aligned} \delta\dot{p}_1 &= -\omega_1 \delta q_1 + G_1 \delta X_c - \gamma_1 \delta p_1 + \xi_1 \\ &- \int_{-\infty}^t g_1(t-s) \delta Y_c^{\text{est}}(s) ds, \end{aligned} \quad (5e)$$

$$\begin{aligned} \delta \dot{p}_2 &= -\omega_2 \delta q_2 + G_2 \delta X_c + G_a \delta X_a - \gamma_2 \delta p_2 + \xi_2 \\ &\quad - \int_{-\infty}^t g_2(t-s) \delta Y_c^{\text{est}}(s) ds \\ &\quad - \int_{-\infty}^t g_a(t-s) \delta Y_a^{\text{est}}(s) ds, \end{aligned} \quad (5f)$$

$$\delta \dot{q}_j = \omega_j \delta p_j. \quad (5g)$$

The applied quantum Langevin equations are equivalent to the standard quantum master equation describing the stationary behavior of the system. It would also be interesting to analyze a generalized method based on, e.g., a feedback quantum master equation like in Ref. [85], which can give another clear insight for the feedback cooling. In Eqs. (5e) and (5f), the convolution term $\int_{-\infty}^t g_j(t-s) \delta Y_c^{\text{est}}(s) ds$ (for $j = 1, 2$) is the cooling-cavity feedback force acting on the j th mechanical mode. In Eq. (5f), the convolution term $\int_{-\infty}^t g_a(t-s) \delta Y_a^{\text{est}}(s) ds$ is the auxiliary-cavity feedback force acting on the second mechanical mode. These feedback forces depend on the past dynamics of the detected quadratures δY_i (for $i = c, a$), which are driven by the weighted sum of the fluctuations of the mechanical modes. The causal kernel is defined by [40,49,51]

$$g_j(t) = g_{\text{cd},j} \frac{d}{dt} [\theta(t) \omega_{\text{fb},j} e^{-\omega_{\text{fb},j} t}], \quad \text{for } j = 1, 2, a, \quad (6)$$

where $\omega_{\text{fb},j}$ and $g_{\text{cd},j}$ are, respectively, the feedback bandwidth and the dimensionless feedback gain. Equation (6) shows the causal kernel, which was applied in a number of works related to cooling (see Refs. [40,49,51]). The estimated intracavity phase quadratures $\delta Y_l^{\text{est}}(s)$ (for $l = c, a$) can be obtained from the homodyne measurement of the output quadrature $Y_{l=c,a}^{\text{out}}(t)$. We generalize the usual input-output relation

$$\delta Y_{l=c,a}^{\text{out}}(t) = \sqrt{2\kappa_l} \delta Y_l(t) - Y_l^{\text{in}}(t) \quad (7)$$

to the case of a nonunit detection efficiency by modeling a detector with quantum efficiency ζ_l with an ideal detector preceded by a beam splitter (with transmissivity $\sqrt{\zeta_l}$), which mixes the incident field with an uncorrelated vacuum field $Y_l^v(t)$. Then, we obtain the generalized input-output relation, which is given by [40,49,51]

$$Y_{l=c,a}^{\text{out}}(t) = \sqrt{\zeta_l} [\sqrt{2\kappa_l} \delta Y_l(t) - Y_l^{\text{in}}(t)] - \sqrt{1-\zeta_l} Y_l^v(t). \quad (8)$$

The estimated phase quadratures $\delta Y_l^{\text{est}}(t)$ are obtained as [40,49,51]

$$\delta Y_{l=c,a}^{\text{est}}(t) = \frac{Y_l^{\text{out}}(t)}{\sqrt{2\zeta_l \kappa_l}} = \delta Y_l(t) - \frac{Y_l^{\text{in}}(t) + \sqrt{\zeta_l^{-1} - 1} Y_l^v(t)}{\sqrt{2\kappa_l}}. \quad (9)$$

Here we highlight that, in principle, the advantage of cold-damping feedback is that it does not require optical cavities because detection via homodyning of the back-scattered light is sufficient to reach the ground state. However, in our work, we focus on the cold-damping feedback cooling based on cavity optomechanical systems, and the optical cavity is necessary for the feedback cooling based on cavity optomechanics. In cavity optomechanical systems, a high sensitivity provided by the cavity readout of mechanical motion can also be used for directly cooling the mechanical motion via active

feedback. The main idea is to obtain the oscillator position by a phase-sensitive detection of the cavity output and to use it to generate a negative feedback on the oscillator, i.e., a force proportional to the time derivative of the output signal. This increases the damping rate of the system without increasing thermal noise (which corresponds to cold damping). Because the scheme relies on the precise readout of the instantaneous oscillator position, the ideal configuration comprises both weak coupling and a fast cavity decay. The maximum amount of cooling is limited by the imprecision of the readout. An important aspect here is the phenomenon of noise squashing where the noise on the detector and the noise-driven motion of the mechanical oscillator become correlated.

Below, we seek the steady-state solution of Eq. (5) by solving it in the frequency domain with a Fourier transformation. We define the Fourier transform for an operator $r(t) = (1/2\pi)^{1/2} \int_{-\infty}^{\infty} e^{-i\omega t} \tilde{r}(\omega) d\omega$ (for $r = \delta X_{a(c)}, \delta Y_{a(c)}, \delta q_{j=1,2}, \delta p_{j=1,2}, \xi_{j=1,2}, X_{a(c)}^{\text{in}}$, and $Y_{a(c)}^{\text{in}}$), and consequently the quantum Langevin equations (5), with the cold-damping feedback, can be solved in the frequency domain. Based on the steady-state solution, we can calculate the spectra of the position and momentum operators for two mechanical modes, and, then, the final mean phonon numbers in these resonators can be obtained by integrating the corresponding fluctuation spectra.

C. Final mean phonon numbers

Mathematically, we can obtain the final steady-state average phonon number in the j th vibrational mode using the following relation [40,63,86]

$$n_{j=1,2}^f = \frac{1}{2} [\langle \delta q_j^2 \rangle + \langle \delta p_j^2 \rangle - 1], \quad (10)$$

where $\langle \delta p_j^2 \rangle$ and $\langle \delta q_j^2 \rangle$ are, respectively, the variances of the momentum and position operators of the j th vibrational mode. By solving Eq. (5) in the frequency domain and integrating the corresponding fluctuation spectra, the variances of the momentum and position operators are

$$\langle \delta q_j^2 \rangle = \frac{1}{2\pi} \int_{-\infty}^{\infty} S_{q_j}(\omega) d\omega, \quad (11a)$$

$$\langle \delta p_j^2 \rangle = \frac{1}{2\pi \omega_j^2} \int_{-\infty}^{\infty} \omega^2 S_{q_j}(\omega) d\omega. \quad (11b)$$

For the corresponding vibrational modes, the fluctuation spectra of the momentum and coordinate operators can be defined by

$$S_o(\omega) = \int_{-\infty}^{\infty} e^{-i\omega\tau} \langle \delta o(t+\tau) \delta o(t) \rangle_{\text{ss}} d\tau, \quad (o = q_j, p_j), \quad (12)$$

where $\langle \cdot \rangle_{\text{ss}}$ is the steady-state mean. In the frequency domain, the fluctuation spectra can be expressed as

$$\langle \delta \tilde{o}(\omega) \delta \tilde{o}'(\omega') \rangle_{\text{ss}} = S_o(\omega) \delta(\omega + \omega'), \quad (o = q_j, p_j). \quad (13)$$

Thus, this system can be solved in the frequency domain. We note that the *exact analytical results of the final mean phonon numbers* are obtained based on Eqs. (10), (11), and (20).

The task of this work is to solve the cooling-suppression obstacle caused by the dark mode by our AFL method. So,

we just need to derive the cooling rates and the mean steady-state phonon numbers, which can be used for studying the cooling performance. Note that the simulations of the cooling dynamics starting with a high-temperature mechanical state is very important too. This is because a simulation of the cooling dynamics could also yield the total cooling time, which could be important information for future experiments.

D. Dark-mode control

Here, we introduce the annihilation (creation) operators for the two mechanical modes $b_j = (q_j + ip_j)/\sqrt{2}$ [$b_j^\dagger = (q_j - ip_j)/\sqrt{2}$], and then study the dark-mode effect in the system. We assume red-detuned cavity fields. Thus, the Hamiltonian in Eq. (5) contains the term describing frequency conversion (i.e., beam-splitter-type interaction), while the two-mode squeezing interaction term can be safely ignored. After performing the linearization, we obtain the linearized Hamiltonian in the rotating-wave approximation (RWA) as

$$H_{\text{RWA}} = \sum_{j=1,2} [\omega_j \delta b_j^\dagger \delta b_j + G_j (\delta d_c \delta b_j^\dagger + \delta d_c^\dagger \delta b_j)] + \sum_{k=c,a} \tilde{\Delta}'_k \delta d_k^\dagger \delta d_k + G_a (\delta d_a \delta b_2^\dagger + \delta d_a^\dagger \delta b_2), \quad (14)$$

where $\tilde{\Delta}'_c$ and $\tilde{\Delta}'_a$ are the normalized driving detunings of the cooling and auxiliary cavities, respectively.

Below, in detail, we discuss the physical system when the auxiliary cavity is absent ($G_a = 0$) and present ($G_a \neq 0$), respectively.

(i) In the absence of the auxiliary device, i.e., $G_a = 0$, the system possesses the dark mode, which leads to inefficient cooling for all the mechanical modes. In this case, the two mechanical modes coupled to a common cavity can form a *bright* mode B_+ and a *dark* mode B_- , which are, respectively, defined as

$$B_+ = \frac{G_1 \delta b_1 + G_2 \delta b_2}{G_0}, \quad \text{Bright}, \quad (15a)$$

$$B_- = \frac{G_2 \delta b_1 - G_1 \delta b_2}{G_0}, \quad \text{Dark}, \quad (15b)$$

where $G_0 = \sqrt{G_1^2 + G_2^2}$. Then, the Hamiltonian in Eq. (14) becomes

$$H_{\text{RWA}} = \tilde{\Delta}'_c \delta d_c^\dagger \delta d_c + \sum_{l=+,-} \omega_l B_l^\dagger B_l + G_+ (\delta d_c B_+^\dagger + \delta d_c^\dagger B_+) + G_- (B_+^\dagger B_- + B_-^\dagger B_+), \quad (16)$$

where $\omega_+ = (\omega_1 G_1^2 + \omega_2 G_2^2)/G_0^2$, $\omega_- = (\omega_1 G_2^2 + \omega_2 G_1^2)/G_0^2$, and the accordingly redefined coupling strengths are given by

$$G_+ = G_0, \quad G_- = \frac{(\omega_1 - \omega_2) G_1 G_2}{G_0^2}. \quad (17)$$

In Fig. 2(a), we plot the redefined coupling strengths G_\pm versus the coupling-strength ratio G_2/G_1 . We find from Fig. 2(a) and Eqs. (16) and (17) that, when $\omega_2 = \omega_1$, the redefined coupling strength G_- is equal to zero (i.e., $G_- = 0$; see the red lines), which indicates that *the mode B_- is decoupled from the system and it becomes a dark mode*; while the redefined coupling strength G_+ is always positive $G_+ > 0$

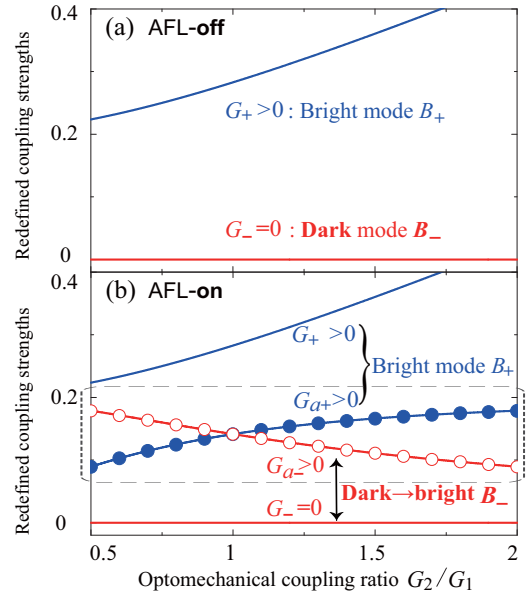


FIG. 2. (a) In the absence of the auxiliary device ($G_a = 0$), the redefined coupling strengths G_+ (blue curve) and G_- (red line) vs the optomechanical coupling ratio G_2/G_1 . (b) The redefined coupling strengths G_\pm and $G_{a,\pm}$ vs the optomechanical coupling ratio G_2/G_1 in the presence of the auxiliary device ($G_a \neq 0$). Here $\omega_2 = \omega_1$ and other parameters are the same as those used in Fig. 1.

(see the blue curves), which means that B_+ is a bright mode. Owing to the presence of the dark mode [6,49,79–82], the cooling of the two mechanical modes is strongly suppressed.

Physically, the two mechanical modes coupled to a common cavity-field mode can be hybridized into a bright mode and a dark mode decoupled from the system. As a result, *the dark mode prevents extracting energy through the cooling channels*, and then the thermal noise, associated with the dark mode, is kept in the system. This means that the dark mode is a major obstacle for multiple-mode cooling in cavity optomechanical systems. Thus, it is naturally to ask the question whether we can control the dark mode to cool these mechanical modes.

(ii) To control this dark mode, an auxiliary device is introduced into the system, i.e., $G_a \neq 0$. By substituting operators B_+ and B_- into the Hamiltonian in Eq. (14), we obtain

$$H_{\text{RWA}} = \sum_{k=c,a} \tilde{\Delta}'_k \delta d_k^\dagger \delta d_k + \sum_{l=+,-} \omega_l B_l^\dagger B_l + G_+ (\delta d_c B_+^\dagger + \delta d_c^\dagger B_+) + G_- (B_+^\dagger B_- + B_-^\dagger B_+) + G_{a+} (\delta d_a B_+^\dagger + \delta d_a^\dagger B_+) - G_{a-} (\delta d_a B_-^\dagger + \delta d_a^\dagger B_-), \quad (18)$$

where we have introduced rescaled coupling strengths $G_{a\pm}$:

$$G_{a\pm} = \chi G_{2(l)}, \quad (19)$$

where $\chi = G_a/G_0$. It can be seen from Eqs. (18) and (19) that, in the presence of the auxiliary device (i.e., $G_a \neq 0$), the two hybrid modes B_+ and B_- are coupled to the system, which means that both B_+ and B_- are bright modes. Physically, the

auxiliary device provides a useful strategy to *couple the dark mode to the system* and, in turn, to rebuild the cooling channel for *extracting the thermal phonons stored in the dark mode*.

In Figs. 2(b), we plot G_{\pm} and $G_{a,\pm}$ versus the coupling-strength ratio G_2/G_1 when $\omega_1 = \omega_2$. We can see that, even though G_- is always equal to zero (see the red lines), the application of the auxiliary device can lead to a strong coupling of the dark mode to the system (i.e., $G_{a,-} > 0$, see the red symbols), which indicates that the dark mode B_- becomes a bright mode. This provides a simple method of *switching between the dark-mode and bright-mode regimes* by using the auxiliary devices.

Here we should highlight that the AFL consists of an auxiliary cavity ($G_a \neq 0$) and an auxiliary cold-damping feedback (CDF) [$g_{cd,a} \neq 0$; see Fig. 1(a)], which are, respectively, used for *controlling the dark mode and generating an auxiliary feedback force* acting on the second mechanical resonator. To realize the feedback cooling of the two mechanical resonators, the system needs the *joint effect* of the auxiliary cavity and the auxiliary CDF. Note that the auxiliary CDF is indispensable to the feedback cooling, and without the auxiliary CDF (i.e., $g_{cd,a} = 0$), the use of the auxiliary cavity (i.e., $G_a \neq 0$) only destroys the dark mode but cannot realize the feedback cooling. Physically, the combination of the auxiliary cavity and the auxiliary CDF does not only break the dark mode but also make the feedback cooling possible.

The main idea behind the proposed method is quite simple. Specifically, if addressing either one of the mechanical modes is made possible, the symmetry of the system is broken and one can control both dark and bright mechanical modes. We believe that the simplicity of this main idea is the advantage of the proposed method rather than its drawback because this indicates a solid physical ground for the predicted giant improvement in cooling efficiency and other related quantities. In particular, our method could solve the outstanding challenge concerning the cooling suppression caused by the mechanical dark mode and pave a way toward dark-mode breaking in multimode optomechanics. Analogously, a well-known method of side-band cooling is also quite simple, as it corresponds to anti-Stokes Raman scattering discovered almost a century ago. That simple and old idea has led to developing and implementing highly nontrivial methods for quantum technologies in recent years.

IV. DOUBLE-MODE OPTOMECHANICAL REFRIGERATION VIA THE AFL

In this section, we study in detail the cooling of the two vibrational modes by analyzing their effective mechanical susceptibilities, laser-cooling rates, and noise spectra.

A. Analytical results of the effective susceptibilities, cooling rates, and noise spectra

In the AFL-on case, the coordinate fluctuation spectra of the two vibrational modes can be obtained as

$$S_{q_1}(\omega) = |\chi_{1,\text{eff}}(\omega)|^2 [S_{\text{fb},1}(\omega) + S_{\text{rp},1}(\omega) + S_{\text{th},1}(\omega)], \quad (20a)$$

$$S_{q_2}(\omega) = |\chi_{2,\text{eff}}(\omega)|^2 [S_{\text{fb},2}(\omega) + S_{\text{rp},2}(\omega) + S_{\text{th},2}(\omega) + S_{\text{fb},a}(\omega) + S_{\text{rp},a}(\omega)]. \quad (20b)$$

Here, we have introduced the *effective susceptibility* of the j th vibrational mode as

$$\chi_{j,\text{eff}}(\omega) = \omega_j [\Omega_{j,\text{eff}}^2(\omega) - \omega^2 - i\omega\Gamma_{j,\text{eff}}(\omega)]^{-1}, \quad (21)$$

where $\Gamma_{j,\text{eff}}(\omega)$ is the *effective mechanical decay rate* and $\Omega_{j,\text{eff}}(\omega)$ is the *effective mechanical resonance frequency* of the j th vibrational mode, which are given by

$$\Gamma_{j,\text{eff}}(\omega) = \gamma_j + \gamma_{j,C}(\omega), \quad (22a)$$

$$\Omega_{j,\text{eff}}(\omega) = \omega_j + \delta\omega_j(\omega). \quad (22b)$$

In Eq. (22a), the *net cooling rates* of the first and second mechanical resonators are

$$\gamma_{1,C} = G_1 g_{cd,1} \omega_1 \omega_{\text{fb},1} \left[-\frac{G_2 g_{cd,2} \omega_2 \omega_{\text{fb},2} E_{15} \omega}{E_{10}^2 + E_{11}^2} + \frac{\kappa_c \omega_{\text{fb},1} - \omega^2}{(\kappa_c + \omega_{\text{fb},1})^2 \omega^2 + (\kappa_c \omega_{\text{fb},1} - \omega^2)^2} \right], \quad (23a)$$

$$\gamma_{2,C} = G_a g_{cd,a} \omega_2 \left\{ \frac{\kappa_a (2\omega^2 + E_4)}{(\kappa_a^2 + \omega^2)^2} - \frac{(\kappa_a A_2 - \omega A_3) \omega}{A_2^2 + A_3^2} \right\} - \frac{G_2 g_{cd,2} \omega_2 \omega_{\text{fb},2} A_{14}}{A_{10}^2 + A_{11}^2}, \quad (23b)$$

and the *mechanical frequency shifts*, induced by the *optical spring effect*, are given by

$$\delta\omega_1 = \sqrt{\omega_1^2 + G_1 g_{cd,1} \omega_1 \omega_{\text{fb},1} \omega^2 \Lambda_1} - \omega_1, \quad (24a)$$

$$\delta\omega_2 = \sqrt{\omega_2^2 + (G_a g_{cd,a} \omega^2 \Lambda_2 - G_2 g_{cd,2} \omega_{\text{fb},2} \Lambda_3) \omega^2} - \omega_2, \quad (24b)$$

where

$$\Lambda_1 = \frac{\kappa_c + \omega_{\text{fb},1}}{(\kappa_c + \omega_{\text{fb},1})^2 \omega^2 + (\kappa_c \omega_{\text{fb},1} - \omega^2)^2} + \frac{G_2 g_{cd,2} \omega_2 \omega_{\text{fb},2} E_{14}}{E_{10}^2 + E_{11}^2}, \quad (25a)$$

$$\Lambda_2 = \frac{\kappa_a A_3 + \omega A_2}{A_2^2 + A_3^2} + \frac{1}{\kappa_a^2 + \omega^2}, \quad (25b)$$

$$\Lambda_3 = \frac{A_{15} \omega}{A_{10}^2 + A_{11}^2}, \quad (25c)$$

and other parameters are presented in the Appendix.

We see from Eqs. (23a) and (24a) that when the feedback loop acting on the first mechanical mode is broken (i.e., $G_1 = 0$ or $g_{cd,1} = 0$), the cooling of the first mechanical mode becomes inefficient (i.e., $\gamma_{1,C} = 0$), and, at the same time, there is no mechanical frequency shift for this resonator (i.e., $\delta\omega_1 = 0$). This indicates that, in the absence of the feedback loop for the first mechanical resonator, the mechanical resonator becomes a dissipative harmonic resonator, i.e., $\Omega_{1,\text{eff}} = \omega_1$ and $\Gamma_{1,\text{eff}} = \gamma_1$. Similarly, for the second mechanical resonator [see Eqs. (23b) and (24b)], due to the breaking of its feedback loops (i.e., $G_a = 0$ or $g_{cd,a} = 0$, and $G_2 = 0$ or $g_{cd,2} = 0$), a dissipative harmonic resonator emerges, i.e., $\Omega_{2,\text{eff}} = \omega_2$ and $\Gamma_{2,\text{eff}} = \gamma_2$.

In Eq. (20), the thermal noise spectrum $S_{\text{th},j}(\omega)$ of the j th mechanical mode is given by

$$S_{\text{th},j}(\omega) = \frac{\gamma_j \omega}{\omega_j} \coth\left(\frac{\hbar \omega}{2k_B T_j}\right). \quad (26)$$

$S_{\text{fb},j}(\omega)$ is the cooling-cavity feedback-induced noise spectrum, and $S_{\text{rp},j}(\omega)$ denotes the cooling-cavity radiation-pressure noise spectrum for the j th mechanical mode. Moreover, $S_{\text{fb},a}(\omega)$ and $S_{\text{rp},a}(\omega)$ denote the auxiliary-cavity feedback-induced noise spectrum and the auxiliary-cavity radiation-pressure noise spectrum for the second mechanical mode, respectively. The analytical expressions of these noise spectra are so complicated that we do not show them here.

B. Giant enhancement of mechanical susceptibilities and net-cooling rates via the AFL

Now, let us study how the AFL largely tunes the effective susceptibilities of the two mechanical modes by analyzing their effective mechanical decay rates $\Gamma_{\text{eff},j}$ and effective mechanical resonance frequencies $\Omega_{\text{eff},j}$.

In both AFL-off [see solid curves in Figs. 1(b) and 1(c)] and AFL-on (see dashed curves) cases, we plot the effective mechanical decay rates $\Gamma_{\text{eff},j}$ and the effective mechanical resonance frequencies $\Omega_{\text{eff},j}$ versus the frequency ω , as shown in Figs. 1(b) and 1(c). We find that owing to the AFL, both $\Gamma_{j,\text{eff}}$ and $\Omega_{j,\text{eff}}$ are significantly increased at resonance $\omega = \pm\omega_m$. For example, when the system operates in the AFL-off case, the effective mechanical decay rates $\Gamma_{\text{eff},j}$ at $\omega = \pm\omega_m$ are equal to $2\gamma_j$, which indicates the two mechanical modes cannot be cooled [see the solid curves in Fig. 1(b)]. In contrast to this, when switching to the AFL-on case, $\Gamma_{\text{eff},j}$ at $\omega = \pm\omega_m$ can be increased from $\approx 2\gamma_j$ to $\gg 10^3\gamma_m$ [see the dashed curves in Fig. 1(b)]. This *giant enhancement in the effective mechanical decay rates* $\Gamma_{\text{eff},j}$ not only makes the *simultaneous cooling* of the two mechanical modes feasible but also could potentially be used for mechanical devices with a large frequency bandwidth.

In addition, we find from Fig. 1(c) that the slight modulation of the mechanical frequencies can be realized by the “*optical spring effect*,” which may lead to the mechanical frequency shifts in the case of low-frequency mechanical resonators. However, for our higher resonance frequencies ($\omega_j/2\pi = 10$ MHz), the optical spring effect does not significantly alter the mechanical frequencies, i.e., $\Omega_{\text{eff},j} \approx \omega_m$ when $\omega/\omega_m = 1$, as shown in Fig. 1(c)].

To further understand the underlying physics of the optomechanical refrigeration under the AFL mechanism, we here study the net-refrigeration rates $\gamma_{j,C}$ and the mechanical resonance frequency shifts $\delta\omega_j$ of the two mechanical modes for the resonance case, i.e., $\omega = \omega_m$. Specifically, we first plot the net-cooling rates $\gamma_{j,C}$ as a function of the coupling strength G_a and the feedback gain $g_{\text{cd},a}$ of the AFL, as shown in Fig. 3. We see that when the AFL is broken ($G_a = 0$ or $g_{\text{cd},a} = 0$), the net-cooling rates of the two mechanical modes are extremely small (i.e., $\gamma_{j,C} \approx \gamma_j$). This results in an inefficient cooling of these mechanical modes, owing to the breaking of the AFL.

When we increase the values of G_a or $g_{\text{cd},a}$, the net-cooling rates $\gamma_{j,C}$ are tremendously amplified, for example, $\gamma_{j,C}$ can be increased from $\gamma_{j,C}/\gamma_j \approx 1$ to $\approx 10^3\text{--}10^4$. In particular, we

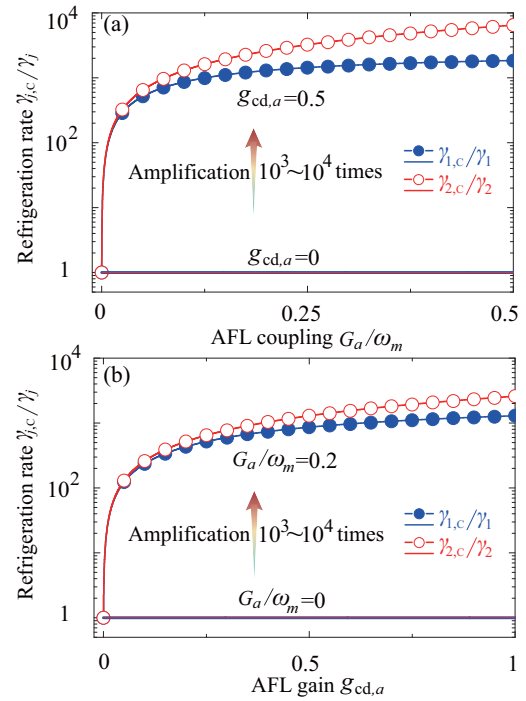


FIG. 3. (a) Net-refrigeration rate $\gamma_{j,C}$ [see Eq. (23)] of the j th vibrational mode versus the AFL-coupling strength G_a , when the AFL-feedback gain $g_{\text{cd},a} = 0.5$. The horizontal solid lines denote an inefficient net-refrigeration rate, when the AFL is broken, i.e., $g_{\text{cd},a} = 0$. (b) Net-refrigeration rate $\gamma_{j,C}$ vs the AFL-feedback gain $g_{\text{cd},a}$, when $G_a = 0.2\omega_m$. The horizontal solid lines denote an inefficient net-refrigeration rate when the AFL is broken, i.e., $G_a = 0$. Here we set the parameter $\omega = \omega_m$, and other parameters are the same as those used in Fig. 1.

find that with increasing either G_a or $g_{\text{cd},a}$, the net-cooling rate of the second mechanical mode is larger than that of the first one, i.e., $\gamma_{1,C} > \gamma_{2,C}$. Physically, the AFL does not only break the dark mode of the system but also offer another cooling channel for the second mechanical mode.

Moreover, we show that by using the AFL mechanism, a slight modulation of the mechanical frequencies emerges. In Fig. 4, the mechanical-frequency shift $\delta\omega_j$ is plotted as a function of the coupling strength G_a or the feedback gain $g_{\text{cd},a}$ of the AFL. We find that in the absence of the AFL mechanism ($g_{\text{cd},a} = 0$ or $G_a = 0$), the mechanical-frequency shift is not induced for the two mechanical modes (i.e., $\delta\omega_{j=1,2} = 0$), while by utilizing the AFL mechanism, a mechanical-frequency shift emerges. However, the resonance frequencies of the two mechanical modes are changed slightly, which is due to a small “optical spring effect” for our high resonance frequencies of the mechanical modes.

C. Dependence of the refrigeration on the cooling-cavity and AFL parameters

The feedback refrigeration of a single mechanical mode in cavity optomechanics is due to the cold-damping effect by a designed feedback force applied to this mechanical mode [40,41,43–51]. Correspondingly, for multiple mechanical modes, in principle, the feedback-assisted refrigeration

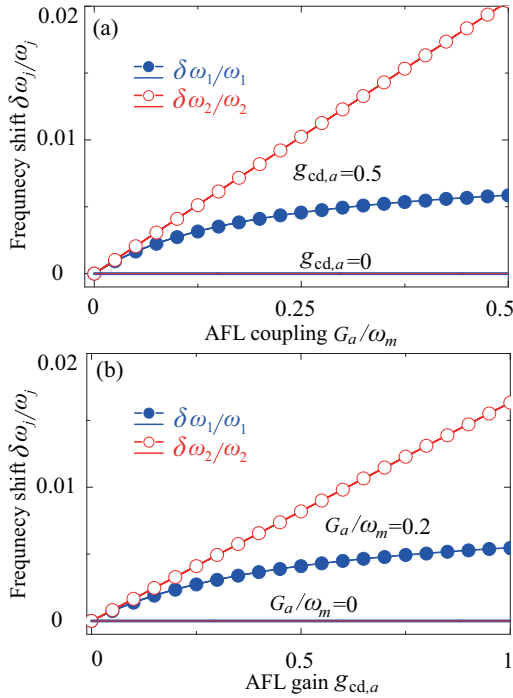


FIG. 4. (a) Mechanical frequency shift $\delta\omega_j$ [see Eq. (24)] of the j th vibrational mode vs the AFL-coupling strength G_a when the AFL-feedback gain $g_{cd,a} = 0.5$. The horizontal solid lines denote the unshifted mechanical frequency when the AFL is broken, i.e., $g_{cd,a} = 0$. (b) $\delta\omega_j$ vs the AFL-feedback gain $g_{cd,a}$ when $G_a = 0.2\omega_m$. The horizontal solid lines denote the unshifted mechanical frequency when the AFL is broken, i.e., $G_a = 0$. Here we take $\omega = \omega_m$, and other parameters are the same as those used in Fig. 1.

mechanism can also lead to their simultaneous refrigeration. However, we find a lack of cooling phenomenon that the multiple mechanical modes coupled to a common cavity-field mode are lack of cooling via the feedback-based refrigeration mechanism. This is because the dark-mode effect, induced by the coupling of the multiple mechanical modes to a common cavity, prevents the extraction of the thermal occupations from the dark mode. *Since this counterintuitive refrigeration results from the dark-mode effect, it is natural to ask whether one can break the dark-mode effect to further cool these mechanical modes to their ground states.* To solve this problem, we use the AFL not only to destroy the dark-mode effect but also to manipulate the cooling performance of these mechanical modes.

In Figs. 5(a) and 5(b), we plot the final steady-state average phonon numbers n_j^f of the j th mechanical mode as a function of the optomechanical coupling strength G_j and the feedback gain $g_{cd,j}$, when the system is in both AFL-off and AFL-on cases. We find that, in the absence of the AFL, the two mechanical modes are uncooled with increasing either G_j or $g_{cd,j}$ (see the upper horizontal lines). The physical origin behind this lack of cooling is that the dark mode decouples from the system and prevents extracting thermal phonons. In contrast, by using the AFL, the ground-state cooling of the two mechanical modes become possible ($n_j^f < 1$; see the dashed curves). Physically, the application of the AFL provides the physical origin for destroying the dark mode and

rebuilding the cooling channels, so that thermal excitations can be extracted.

In particular, it is shown that in the AFL-on case, the cooling performance of the second mechanical mode is much better than that of the first one, with increasing either G_j or $g_{cd,j}$ [see the dashed curves in Figs. 5(a) and 5(b)]. The optimal cooling performances of the two mechanical modes can be achieved for the parameters $0.2 \leq G_j/\omega_j \leq 0.4$ and $0.25 \leq g_{cd,j} \leq 1$. However, when $G_j \rightarrow 0$ or $g_{cd,j} \rightarrow 0$, the first mechanical modes cannot be cooled because of the breaking of its feedback loop, while the second one still can be cooled. This is because the AFL is always applied on the second resonator and provides another cooling channel to extract its thermal phonons.

When the system operates in the AFL-off [see the upper horizontal lines in Fig. 5(c)] and AFL-on (see the dashed curves) cases, the steady-state average phonon number n_j^f is plotted as a function of the cooling-cavity feedback bandwidth $\omega_{fb,j}$, as shown in Fig. 5(c). We see that, for the AFL-off case, the cooling of the two mechanical modes is totally inefficient, while for the AFL-on case, the ground-state cooling is possible ($n_1^f, n_2^f < 1$). Furthermore, we find that the optimal cooling of the two mechanical modes is achieved when $\omega_{fb,j}/\omega_m \approx 4$. When we decrease the cooling-cavity feedback bandwidth, i.e., $\omega_{fb,j} \rightarrow 0$, the cooling efficiency of the two mechanical modes becomes much lower. Physically, a lower feedback bandwidth, corresponding to a longer time delay of the feedback loop, leads to a lower cooling efficiency of the mechanical modes.

Since the AFL mechanism plays a crucial role in destroying the dark mode and rebuilding the cooling channels of the system, the dependence of the cooling performance of these mechanical modes on the parameters of the AFL mechanism should be studied in detail.

In the AFL-on case, we plot the thermal phonon number n_j^f as a function of the AFL coupling strength G_a and the AFL feedback gain $g_{cd,a}$, as shown in Figs. 5(d) and 5(e), respectively. It can be seen that when we turn on the AFL ($G_a \neq 0$ and $g_{cd,a} \neq 0$), the two mechanical modes can be cooled to their quantum ground states efficiently ($n_j^f < 1$) due to the breaking of the dark mode; while when turning off the AFL ($G_a = 0$ or $g_{cd,a} = 0$), they cannot be cooled because of the emergence of the dark mode. In addition, we find that the cooling efficiency of the second mechanical mode is much better than that of the first one under proper parameter conditions and that the optimal refrigeration performances can be observed for $0.2 \leq G_a/\omega_m \leq 0.6$ and $0.4 \leq g_{cd,a} \leq 1.5$. The resulting asymmetrical ground-state cooling is due to the fact that the AFL exerted on the second mechanical mode provides another cooling channel for extracting the thermal phonons of the second mechanical mode.

Surprisingly, there exists one cooling switch point (i.e., $n_1^f = n_2^f$) in Fig. 5(e). This phenomenon indicates that by appropriately engineering the AFL, a flexible asymmetric-to-symmetric or symmetric-to-asymmetric cooling switch can be achieved. Moreover, we show that when $G_a/\omega_m < 0.2$ and $g_{cd,a} < 0.5$, the refrigeration performance becomes less efficient by decreasing G_a and $g_{cd,a}$. These findings mean that the AFL plays a crucial role of the dark-mode breaking

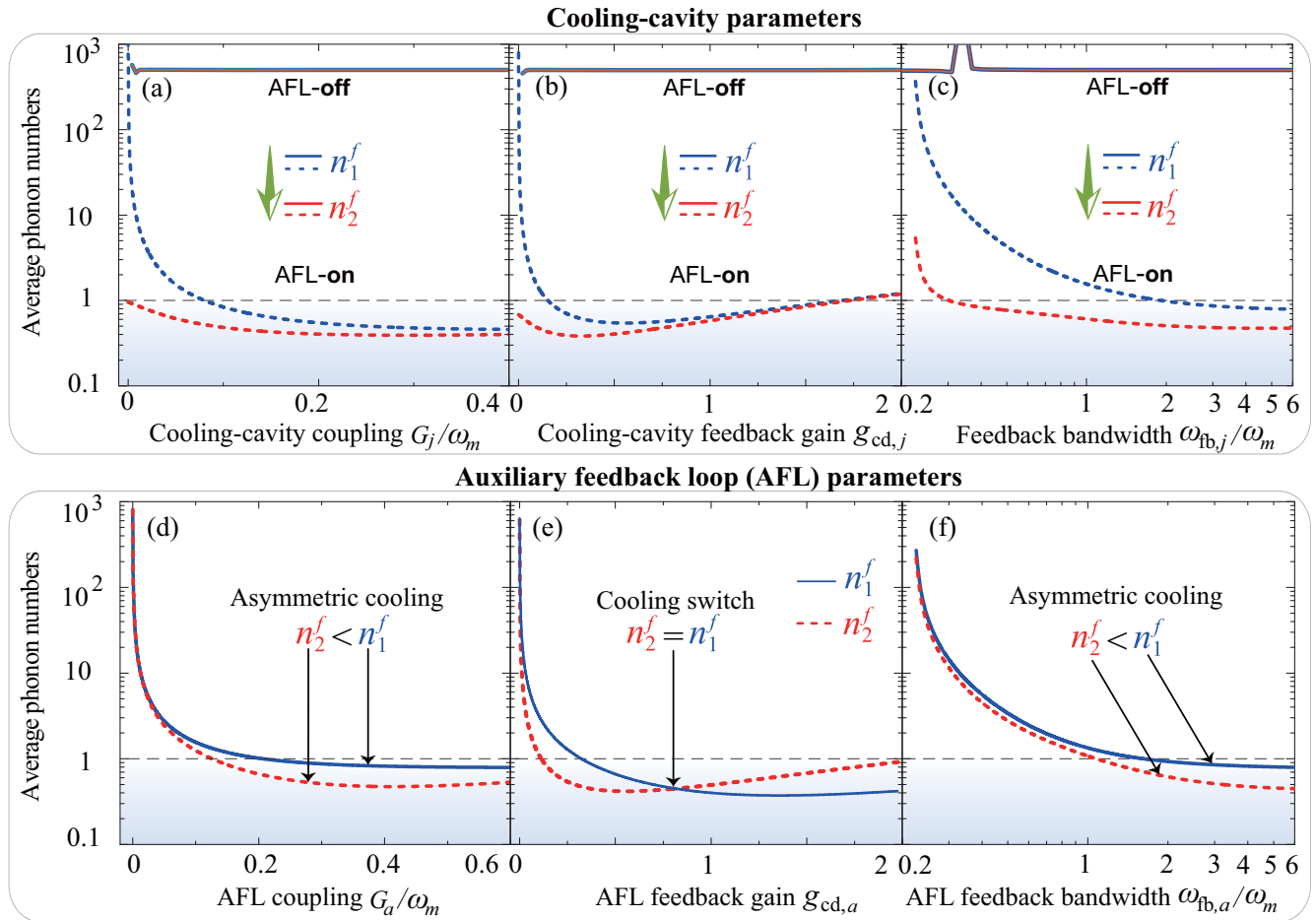


FIG. 5. [(a)–(c)] Final steady-state mean phonon numbers, n_1^f and n_2^f , of the two mechanical modes vs (a) the cooling-cavity optomechanical coupling strength G_j , (b) the cooling-cavity feedback gain $g_{cd,j}$, and (c) the cooling-cavity feedback bandwidth $\omega_{fb,j}$, when the system is in the AFL-off ($G_a/\omega_m = 0$ and $g_{cd,a} = 0$, upper horizontal solid lines) and AFL-on ($G_a/\omega_m = 0.4$ and $g_{cd,a} = 0.5$, dashed curves) cases. [(d)–(f)] In the AFL-on case, n_1^f (blue solid curves) and n_2^f (red dashed curves) are plotted vs (d) the AFL optomechanical coupling strength G_a , (e) the AFL feedback gain $g_{cd,a}$, and (f) the AFL feedback bandwidth $\omega_{fb,a}$. Other parameters are the same as in Fig. 1.

and the cooling impetus and that all the mechanical modes are uncooled when the AFL is broken (i.e., $G_a/\omega_m \rightarrow 0$ or $g_{cd,a} \rightarrow 0$). This is because the reappearance of the dark-mode effect breaks the cooling channels.

In addition, the cooling performance of the two mechanical modes is plotted as a function of the feedback bandwidth $\omega_{fb,a}$ of the AFL, as shown in Fig. 5(f). It is shown that (i) the optimal cooling performance of the two mechanical modes can be observed for $\omega_{fb,a}/\omega_m \geq 3$ and that (ii) the cooling of the two mechanical modes becomes inefficient when $\omega_{fb,a} \rightarrow 0$. This is because a lower feedback bandwidth indicates a longer time delay of the feedback loop, resulting in a lower cooling efficiency for the two mechanical modes.

In Fig. 6, we plot the final mean steady-state phonon numbers n_1^f (see blue symbols) and n_2^f (see red symbols) versus the cooling-cavity decay rate κ_c and the AFL-cavity decay rate κ_a , when the system operates in the AFL-on case. We find that with decreasing either κ_c or κ_a , the cooling efficiencies of the two mechanical modes become much lower in the resolved-sideband regimes and that the ground-state cooling can be achieved ($n_1^f, n_2^f < 1$) in the unresolved-sideband regimes: $\kappa_c/\omega_m > 1$ and $\kappa_a/\omega_m > 1$. On the other hand, the

optimal cooling of the two mechanical modes is achieved for $\kappa_c/\omega_m > 2$ and $\kappa_a/\omega_m > 2$. Our unresolved-sideband cooling results are fundamentally different from those in the sideband cooling, for which the optimal cooling is reached only in the resolved-sideband regime [38,39,66].

Moreover, it is worth comparing the cooling rates of the two mechanical modes (with the AFL on) with the cooling rate of the second mechanical mode when the first mechanical mode is decoupled from the main optical cavity, i.e., with $G_1 = 0$ and $G_{cd,1} = 0$.

To illustrate this point, we plot the net-cooling rates $\gamma_{j,c}$ of the j th mechanical mode versus the AFL-coupling strength G_a , when the first mechanical mode is present ($G_1 \neq 0$ and $G_{cd,1} \neq 0$, see the solid curves) and absent ($G_1 = 0$ and $G_{cd,1} = 0$, see the dashed curves), as shown in Fig. 7. In the absence of the first mechanical mode, the net cooling rates of the two mechanical modes are much larger than their mechanical damping rates (i.e., $\gamma_{j,c} \gg \gamma_j$), which means that both mechanical modes can be efficiently cooled to their quantum ground states. In particular, we see that when we increase the value of G_a , the net-cooling rate of the second mechanical mode is larger than that of the first one, i.e., $\gamma_{1,c} > \gamma_{2,c}$.

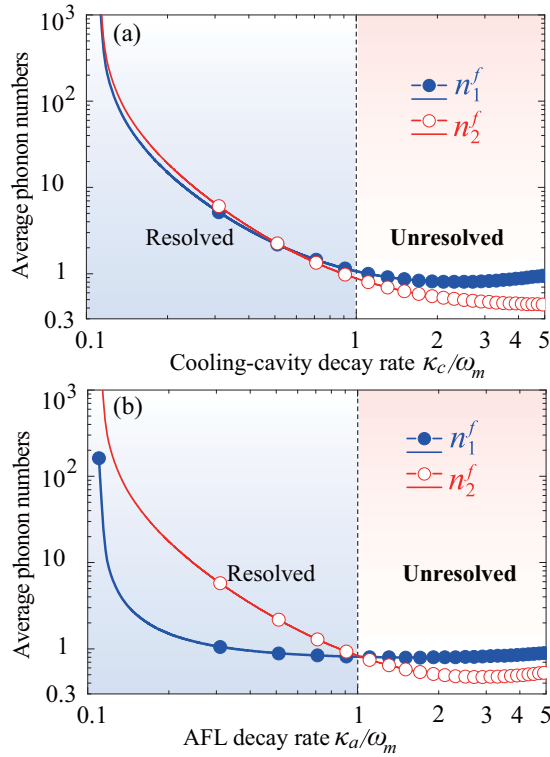


FIG. 6. In the presence of the AFL, the final steady-state average phonon numbers n_1^f (blue) and n_2^f (red) vs (a) the cooling-cavity decay rate κ_c when $\kappa_a = 3\omega_m$ and (b) the AFL decay rate κ_a when $\kappa_c = 3\omega_m$. Other parameters are the same as those used in Fig. 1.

Physically, the AFL plays a role not only in breaking the dark mode of the system, but also in opening another cooling channel for the second mechanical mode. In the absence of the first mechanical mode, we find that the cooling rate of the first mode is equal to zero due to the breaking of its cooling channel, while the cooling rate of the second mechanical mode is larger than that in the case where the first mechanical mode is present. In conclusion, these results indicate that by

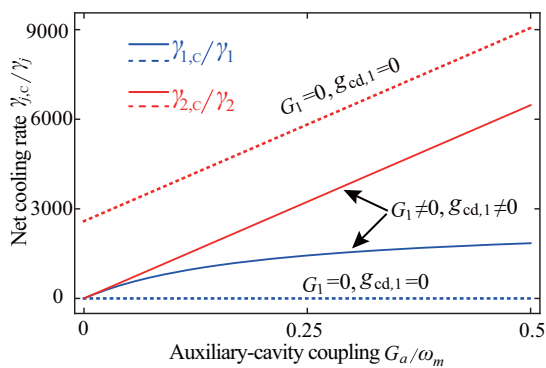


FIG. 7. Net-refrigeration rates $\gamma_{1,c}$ (blue curves) and $\gamma_{2,c}$ (red curves) vs the AFL-coupling strength G_a , when the first mechanical mode is present ($G_1 \neq 0$ and $G_{cd,1} \neq 0$, see the solid curves) and absent ($G_1 = 0$ and $G_{cd,1} = 0$, see the dashed curves). Here we set the parameter $\omega = \omega_m$, and other parameters are the same as those used in Fig. 1.

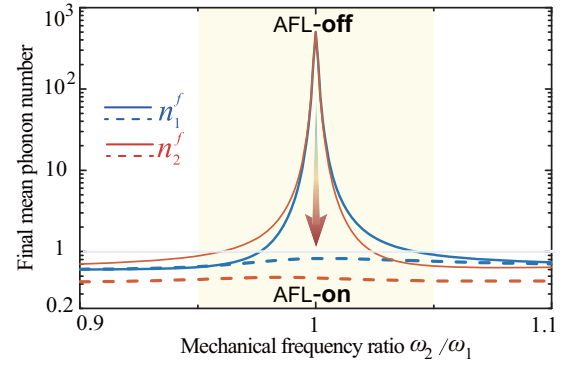


FIG. 8. The final mean phonon numbers n_1^f (blue curves) and n_2^f (red curves) as functions of the mechanical frequency ratio ω_2/ω_1 for the AFL-off (solid curves) and AFL-on (dashed curves) cases. Other parameters are the same as those used in Fig. 1.

introducing the AFL to a typical optomechanical system, the net-cooling rate of the resonator can be largely enhanced, and this is crucial for developing the cooling performance of the system.

We note that although the dark mode exists theoretically only in the degenerate-resonator case, i.e., $\omega_1 = \omega_2$, the dark-mode effect, induced by this dark mode, actually works within a finite mechanical detuning range in the near-degenerate-resonator case. To know the width of the frequency-detuning window associated with this dark-mode effect, in Fig. 8 we show the final average phonon numbers n_1^f and n_2^f as functions of the mechanical frequency ratio ω_2/ω_1 in both AFL-off (see the solid curves) and AFL-on (see the dashed curves) cases. For the AFL-off case, the ground-state cooling of the two mechanical modes is unfeasible in both degenerate and near-degenerate-resonator cases, as marked by the shadow area. The width of the shadow area can be characterized by the effective mechanical linewidth, $|\omega_2 - \omega_1| \leq \Gamma_{j,\text{eff}}$. This is because the cooling of the two mechanical resonators is strongly suppressed in this region, and thus the two mechanical resonators have a significant spectral overlap and become effectively degenerate.

However, when the AFL is introduced to the system (see the dashed curves in Fig. 8), the dark-mode effect is completely broken, and the ground-state cooling of these mechanical modes can be realized irrespective of the value of the ratio ω_2/ω_1 . These results indicate that both degenerate and near-degenerate vibrational modes can be cooled to their quantum ground states and that our method can solve the cooling suppression obstacle for both near-degenerate and degenerate cases.

The dark modes in cavity optomechanics can be divided into (i) mechanical and (ii) optical dark modes. Physically, the mechanical (optical) dark modes are induced by the coupling of multiple mechanical (optical) modes to a common optical (mechanical) mode. The mechanical dark modes are governed by the mechanical-frequency detuning (i.e., $\omega_2 - \omega_1$) between the resonators. They are formed when the mechanical-frequency detuning is equal to zero (i.e., $\omega_2 - \omega_1 = 0$) and are suppressed when the mechanical-frequency detuning is nonzero (i.e., $\omega_2 - \omega_1 \neq 0$).

Similarly, for the optical dark modes, their formations are directly decided by the driving-detuning difference between the optical modes. The zero value of the driving-detuning difference leads to the creation of the optical dark modes, and the suppression of the formation of the dark mode is caused by a nonzero value of the driving-detuning difference between the optical modes. In this work, we focus only on studying the effect of the mechanical dark mode on the cooling performance of the mechanical modes. In Fig. 8, we demonstrate that although the mechanical dark mode exists theoretically only for the zero-value mechanical detuning (i.e., $\omega_1 = \omega_2$), the dark-mode effect actually will be worked for a wide detuning range (i.e., $\omega_1 \neq \omega_2$; see the shadow region in Fig. 8). In the following section, we will study the optical-dark-mode effect of the system in detail.

V. OPTICAL DARK MODE, OPTIMAL FEEDBACK PARAMETERS, AND DISCUSSION

A. Optical dark mode

In the system, there also exists an optical dark mode formed by the two optical modes coupled to a common mechanical mode. For demonstrating the optical dark mode, we here consider the case where the main and auxiliary optical modes couple to a mechanical mode; i.e., we set $G_1 = 0$ and $g_{cd,1} = 0$ in Eq. (5). Then, the two optical modes can form the optical bright mode D_+ and the optical dark mode D_- , which are given by

$$D_+ = \frac{G_2 \delta d_c + G_a \delta d_a}{\tilde{G}_0}, \quad \text{Optical bright mode}, \quad (27a)$$

$$D_- = \frac{G_a \delta d_c - G_2 \delta d_a}{\tilde{G}_0}, \quad \text{Optical dark mode}, \quad (27b)$$

where $\tilde{G}_0 = \sqrt{G_2^2 + G_a^2}$. Then, the Hamiltonian in Eq. (5) can be rewritten as

$$H_{\text{RWA}} = \sum_{j=\pm} \tilde{\Delta}_j D_j^\dagger D_j + \omega_2 \delta b_2^\dagger \delta b_2 + \tilde{G}_+ (\delta b_2 D_+^\dagger + D_+ \delta b_2^\dagger) + \tilde{G}_- (D_+^\dagger D_- + D_-^\dagger D_+), \quad (28)$$

where $\tilde{\Delta}_{+(-)} = [G_2^2 \tilde{\Delta}'_c + G_a^2 \tilde{\Delta}'_a] / \tilde{G}_0^2$ and the coupling strengths are

$$\tilde{G}_- = \frac{G_2 G_a (\tilde{\Delta}'_c - \tilde{\Delta}'_a)}{\tilde{G}_0^2}, \quad \tilde{G}_+ = \tilde{G}_0. \quad (29)$$

We can see from Eqs. (28) and (29) that when $\tilde{\Delta}'_c = \tilde{\Delta}'_a$, the mode D_- is decoupled from the system due to $\tilde{G}_- = 0$, and it becomes an optical dark mode. Similar to the mechanical dark mode, the formation of the optical dark mode is decided by the driving-detuning difference (i.e., $\tilde{\Delta}'_c - \tilde{\Delta}'_a$) between the two optical modes. We find that when the detuning difference is equal to zero ($\tilde{\Delta}'_c - \tilde{\Delta}'_a = 0$), the optical dark mode emerges and that the suppression of the formation of the dark mode occurs when this difference is nonzero ($\tilde{\Delta}'_c - \tilde{\Delta}'_a \neq 0$).

B. Optimal feedback parameters

How to practically choose the feedback bandwidths and gains is very crucial for achieving the fastest cooling and

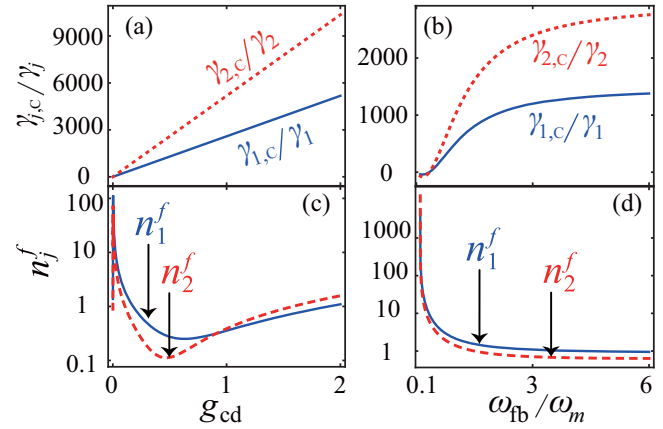


FIG. 9. Net-refrigeration rate $\gamma_{j,c}$ of the j th vibrational mode vs (a) the feedback gain g_{cd} and (b) the feedback sideband ω_{fb} . The final mean phonon numbers n_j^f of the j th vibrational mode vs (c) the feedback gain g_{cd} and (d) the feedback sideband ω_{fb} . Here we set the parameter $\omega = \omega_m$, and other parameters are the same as those used in Fig. 1.

lowest stationary occupation. To know the optimal feedback parameters, we considered the case of $g_{cd,j} = g_{cd,a} = g_{cd}$ and $\omega_{cd,j} = \omega_{cd,a} = \omega_{cd}$, and then plotted the net-cooling rates $\gamma_{j,c}$ and the final mean phonon numbers n_j^f of the j th mechanical mode (for $j = 1, 2$) as functions of the feedback gain g_{cd} and the feedback bandwidth ω_{fb} , as shown in Fig. 9.

One can see from Figs. 9(a) and 9(b) that the net-cooling rates can be significantly improved by increasing either g_{cd} or ω_{fb} , and that the optimal feedback bandwidth can be observed for $\omega_{fb}/\omega_m > 3$. In addition, we can see that the net-cooling rate of the second mechanical mode is always much larger than that of the first one. Moreover, the optimal cooling performance (i.e., the lowest stationary occupation) of the two vibrational modes is located in the areas $g_{cd} \approx 0.5$ and $\omega_{fb}/\omega_m > 3$, as shown in Figs. 9(c) and 9(d). In particular, we find that under proper parameter conditions, the cooling performance of the second resonator is better than that of the first one, and this can be explained by the fact that the AFL offers another cooling channel for the second resonator.

C. Discussion

Here we discuss the cooling case, where the auxiliary-cavity driving detuning is not equal to zero, i.e., $\Delta_a \neq 0$. In Fig. 10, we plot the net cooling rate $\gamma_{j,c}$ of the j th mechanical mode as a function of the auxiliary-cavity driving detuning Δ_a , when the AFL is turned on. Here we choose the mechanical frequency ω_m as the frequency scale, so that we can clearly see the relationship between the optimal driving detunings. We see that by introducing the AFL, the net-cooling rates $\gamma_{j,c}$ of the two mechanical modes are much larger than their mechanical decays (i.e., $\gamma_{j,c} \gg \gamma_m$), which means that the simultaneous ground-state cooling is achievable in this system. In particular, we find that the peak values of the net-cooling rates emerge when $\Delta_a = 0$, and net-cooling rates become smaller with the increase of the auxiliary-cavity detuning Δ_a . This is because the highest sensitivity for the position

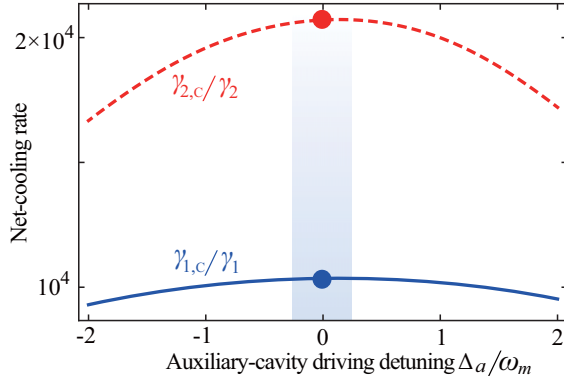


FIG. 10. Net-refrigeration rates $\gamma_{1,c}$ (blue solid curves) and $\gamma_{2,c}$ (red dashed curves) vs the auxiliary-cavity driving detuning Δ_a , when the AFL is present. Here we set the parameters $\omega = \omega_m$ and $g_{cd,j} = g_{cd,a} = 4$, and other parameters are the same as those used in Fig. 1.

measurements can be achieved for a resonant cavity (i.e., $\Delta_a = 0$) and in the large-cavity bandwidth limit $\kappa \gg \omega_m$.

VI. GENERALIZATION TO THE LOOP-COUPLED SYSTEM AND POSSIBLE EXPERIMENTAL REALIZATIONS

Here, we extend our method to a loop-coupled system, where the auxiliary cavity is coupled to both mechanical modes. When the system is driven by the red-detuned lasers, the linearization scheme can be performed to simplify the system, and thus the linearized Hamiltonian in the RWA reads

$$H_{\text{RWA}} = \sum_{j=1,2} [\omega_j \delta b_j^\dagger \delta b_j + G_j (\delta d_c \delta b_j^\dagger + \delta d_c^\dagger \delta b_j)] + \tilde{\Delta}'_c \delta d_c^\dagger \delta d_c + \tilde{\Delta}'_a \delta d_a^\dagger \delta d_a + G_a (\delta d_a \delta b_2^\dagger + \delta d_a^\dagger \delta b_2) + G_{a1} (\delta d_a \delta b_1^\dagger + \delta d_a^\dagger \delta b_1), \quad (30)$$

where G_{a1} (G_a) is the effective optomechanical coupling strength between the first (second) mechanical mode and the auxiliary cavity-field mode. By considering the degenerate-resonator case (i.e., $\omega_1 = \omega_2$) and by substituting the operators B_\pm [see Eq. (15)] into the Hamiltonian in Eq. (30), we obtain

$$H_{\text{RWA}} = \tilde{\Delta}'_c \delta d_c^\dagger \delta d_c + \tilde{\Delta}'_a \delta d_a^\dagger \delta d_a + \sum_{l=+,-} \omega_l B_l^\dagger B_l + G_+ (\delta d_c B_+^\dagger + \delta d_c^\dagger B_+) + (G_{a1+} + G_{a+}) (\delta d_a B_+^\dagger + \delta d_a^\dagger B_+) + (G_{a1-} - G_{a-}) (\delta d_a B_-^\dagger + \delta d_a^\dagger B_-), \quad (31)$$

where $G_{a1\pm}$ is introduced rescaled coupling strength, defined as

$$G_{a1+(-)} = \chi_1 G_{1(2)}, \quad (32)$$

with $\chi_1 = G_{a1}/G_0$. In Fig. 11, we plot the redefined effective optomechanical coupling strength G_+ (the black dashed line), $(G_{a1+} + G_{a+})$ (the red dotted line), and $|G_{a1-} - G_{a-}|$ (the red solid line) as functions of the auxiliary-cavity op-

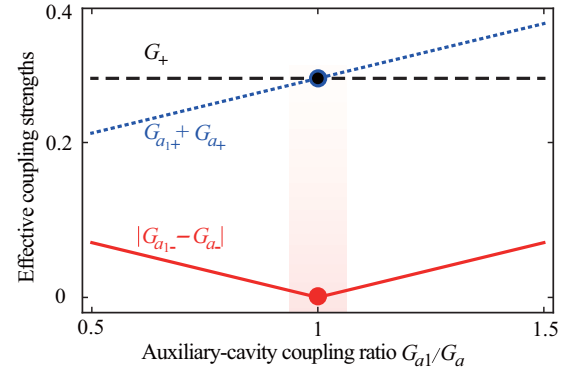


FIG. 11. Redefined effective coupling strengths G_+ (black dashed line), $(G_{a1+} + G_{a+})$ (red dotted line), and $|G_{a1-} - G_{a-}|$ (red solid line) vs the auxiliary-cavity optomechanical coupling ratio G_{a1}/G_a . Here we assume $G_a/\omega_m = 0.2$, and other parameters are the same as those used in Fig. 1.

tomachanical coupling ratio G_{a1}/G_a . It can be seen that by tuning the coupling ratio G_{a1}/G_a , the coupling strengths G_+ and $(G_{a1+} + G_{a+})$ are always nonzero, which indicates that the mode B_+ is a bright mode. In contrast to this, when $G_{a1} = G_a$, we obtain the coupling strength $G_{a1-} - G_{a-} = 0$, and this means that the mode B_- is decoupled from the system and becomes a dark mode. Thus, the excitation energy stored in the dark mode cannot be extracted through the optomechanical-cooling channel. For the general case of $G_{a1} \neq G_a$, the dark-mode effect is broken, and thus the ground-state cooling of the two mechanical resonators becomes feasible under proper parameter conditions.

Now, let us discuss possible experimental realizations of this loop-coupled optomechanical system. In the microwave domain, this system can be realized using a superconducting circuit [87], which consists of two microwave cavities and two vibrational modes, as shown in Fig. 12(a). Specifically, two microwave cavities can be defined by combining a vacuum-gap capacitor with an inductive network. The vacuum-gap capacitor has a mechanically compliant top plate that vibrates with several spectrally distinct mode frequencies, corresponding to different vibrational modes. Furthermore, one can experimentally realize the system using another superconducting circuit optomechanical system [88], where the mechanical motions are capacitively coupled to a multimode microwave circuit, as shown in Fig. 12(b). The circuit supports two optical modes, both of them coupled to the same vacuum-gap capacitor, and the two microwave cavities are symmetrically coupled to the mechanical modes. In the optical domain, this system can be realized by using a multimode optomechanical cavity [30], where two optical modes are coupled to two mechanical modes. To prevent cross-mode interactions, the two optical modes are chosen to be well separated.

When we turn off the coupling channel between the auxiliary-cavity mode and the first mechanical mode, the loop-coupled system (see Fig. 12) reduces the system shown in Fig. 1. Here, we present some discussions on the experimental realization of our model, when the auxiliary cavity couples only to the second mechanical mode. In the optical domain, this system can be realized based on the

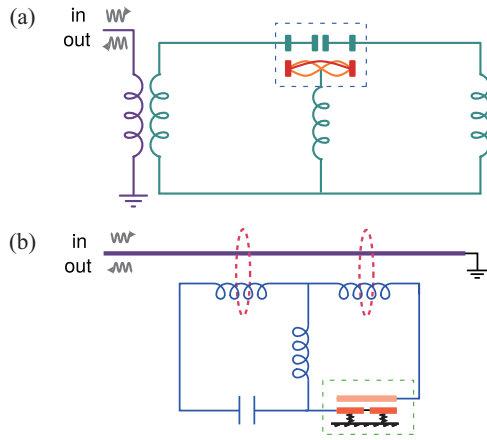


FIG. 12. (a) Schematic of the optomechanical circuit consisting of two microwave cavities and two vibrational modes. Two microwave cavities are defined by combining a vacuum-gap capacitor with an inductive network, and the vacuum-gap capacitor has a mechanically compliant top plate that vibrates with several spectrally distinct mode frequencies, i.e., the vibrational modes. (b) Implementation of a superconducting microwave circuit optomechanical device. A superconducting circuit featuring two electromagnetic modes in the microwave domain is capacitively coupled to a mechanical element (a vacuum-gap capacitor denoted by dashed rectangle) and inductively coupled to a microstrip feedline. The end of the feedline is grounded and the circuit is measured via black-scattered light.

Fabry-Prot-cavity optomechanical configurations, which consist of a double-movable-mirror optomechanical cavity coupled to another cavity field, as shown Fig. 13. In this system, the two mechanical resonators $q_{j=1,2}$ are coupled to a common cooling cavity d_c via the radiation-pressure couplings of strengths G_j . An auxiliary cavity d_a is coupled to the second mechanical resonator q_2 via an optomechanical coupling of

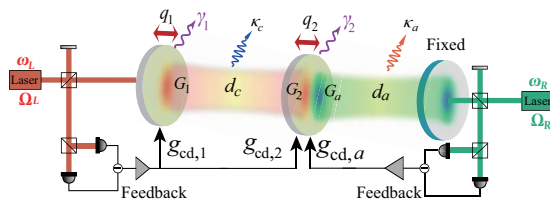


FIG. 13. Implementation of a multimode optomechanical system using the Fabry-Prot-cavity optomechanical configuration consisting of a double-movable-mirror optomechanical cavity (d_c) coupled to another cavity field (d_a). The cooling-cavity mode d_c (with resonance frequency ω_c and cavity-field decay rate κ_c) is coupled to the two mechanical resonators $q_{j=1,2}$ (both with resonance frequency ω_m and mechanical decay rate γ_j) through the radiation-pressure couplings of strengths G_j . The second mechanical resonator q_2 is also coupled to the auxiliary cavity d_a (with resonance frequency ω_a and cavity-field decay rate κ_a) via an optomechanical coupling G_a . The output fields of the two driven cavities are measured via homodyne detection and then the feedback loops (with optomechanical couplings $G_{k=1,2,a}$ and feedback gains $g_{cd,k=1,2,a}$) are utilized to design direct forces exerted on the two mechanical resonators. This leads to the freezing of their thermal fluctuations (i.e., the cold-damping effect) [40–51].

the strength G_a . The homodyne detection is used for measuring the output fields of the two driven cavities and then the direct forces exerted on the two mechanical resonators are designed by utilizing the feedback loops, which can lead to the freezing of their thermal fluctuations (i.e., the cold-damping effect) [40–51].

The proposed physical model is general, and hence, it can be implemented using cavity optomechanical platforms in which the involved interactions can be realized. To implement the dark-mode-breaking multimode cooling by the auxiliary feedback loop, three important ingredients are required: (a) The first and second mechanical modes can be coupled to the first optical mode; (b) the second mechanical mode can be coupled to the second optical mode; and (c) the distinct homogeneous feedback forces can be applied to both mechanical modes. Therefore, these three elements should be implementable in our candidate experimental systems. It should be pointed out that although these three ingredients have been realized in separate experiments, the implementation of the combination of these three requirements in the same experimental setup has not been experimentally reported yet. This is a potential experimental challenge in realistic experimental setups. However, we believe that this challenge can be overcome in the near future.

VII. CONCLUSION

In conclusion, we have solved the outstanding challenge of cooling suppression from mechanical dark modes in cavity optomechanics and shown how to simultaneously cool two vibrational modes to their quantum ground states beyond the resolved-sideband regime by breaking the dark mode via an AFL. We have found that using our AFL method can lead to a flexible switch between the dark-mode-breaking and dark-mode-unbreaking regimes. Our method can lead to a giant amplification in the net-cooling rates and the effective mechanical susceptibilities of the two vibrational modes, and this can be used for significantly developing the cooling performance of these vibrational modes. Remarkably, we find that in the absence of the AFL, all the mechanical modes are uncooled due to the dark mode, while by introducing the AFL, the simultaneous ground-state refrigeration becomes feasible because of the dark-mode breaking.

In addition, we have shown that the refrigeration performance of the two mechanical modes can be flexibly switched between the symmetric-cooling and asymmetric-cooling regimes, by appropriately engineering the feedback gain of the AFL. Our work could potentially be used for expanding the frequency bandwidth of mechanical devices, observing quantum mechanical effects, and manipulating macroscopic mechanical coherence.

ACKNOWLEDGMENTS

A.M. is supported by the Polish National Science Centre (NCN) under the Maestro Grant No. DEC-2019/34/A/ST2/00081. F.N. is supported in part by Nippon Telegraph and Telephone Corporation (NTT) Research, the Japan Science and Technology Agency (JST) [via the Quantum Leap Flagship Program (Q-LEAP) program, the

Moonshot R&D Grant No. JPMJMS2061], the Japan Society for the Promotion of Science (JSPS) [via the Grants-in-Aid for Scientific Research (KAKENHI) Grant No. JP20H00134], the Army Research Office (ARO) (Grant No. W911NF-

18-1-0358), the Asian Office of Aerospace Research and Development (AOARD) (via Grant No. FA2386-20-1-4069), and the Foundational Questions Institute Fund (FQXi) via Grant No. FQXi-IAF19-06.

APPENDIX: ANALYTICAL EXPRESSIONS OF THE STEADY-STATE MEAN PHONON NUMBER

In this Appendix, we show the expressions of other parameters used in Eqs. (23)–(25). These expressions are given by

$$\begin{aligned}
A_1 &= (\omega^2 - \omega_{\text{fb},2}\omega_{\text{fb},a})\kappa_c + (\omega_{\text{fb},a} + \omega_{\text{fb},2})\omega^2, & A_2 &= [E_4 + 2\kappa_a\omega_{\text{fb},a}]\omega, \\
A_3 &= E_4\omega_{\text{fb},a} - 2\kappa_a\omega^2, & A_4 &= \kappa_c(\omega^2 - \omega_1^2) + \gamma_1\omega^2, & A_5 &= [\kappa_c\gamma_1 - (\omega^2 - \omega_1^2)]\omega, \\
A_6 &= \kappa_c\gamma_1 - \omega^2, & A_7 &= (\kappa_c + \gamma_1)\omega, & A_8 &= (A_6 + \omega_1^2 + G_1g_{\text{cd},1}\omega_1)\omega_{\text{fb},1}\omega, \\
A_9 &= (\kappa_c\omega_1^2 - A_7\omega)\omega_{\text{fb},1}, & A_{10} &= (\omega A_4 - A_8)\omega - (\omega A_5 - A_9)\omega_{\text{fb},2}, \\
A_{11} &= (\omega A_4 - A_8)\omega_{\text{fb},2} + (\omega A_5 - A_9)\omega, & A_{12} &= \gamma_1\omega^2 + (\omega^2 - \omega_1^2)\omega_{\text{fb},1}, \\
A_{13} &= [\gamma_1\omega_{\text{fb},1} - (\omega^2 - \omega_1^2)]\omega, & A_{14} &= A_{12}A_{10} + A_{13}A_{11}, \\
A_{15} &= A_{13}A_{10} - A_{12}A_{11}, & B_1 &= [(\omega_{\text{fb},a} + \omega_{\text{fb},2})\kappa_c - (\omega^2 - \omega_{\text{fb},2}\omega_{\text{fb},a})]\omega, \\
C_1 &= [-E_4 - 2\kappa_a\omega_{\text{fb},a}]\omega, & D_1 &= 2\kappa_a\omega^2 - E_4\omega_{\text{fb},a}, \\
E_1 &= (\omega^2 - \kappa_a\kappa_c)\omega - (\kappa_a + \kappa_c)\omega_{\text{fb},2}\omega, & F_5 &= \omega^2 - \kappa_c\omega_{\text{fb},1},
\end{aligned} \tag{A1}$$

and

$$\begin{aligned}
F_1 &= (\omega^2 - \kappa_a\kappa_c)\omega_{\text{fb},2} + (\kappa_a + \kappa_c)\omega^2, & F_2 &= E_4\omega_2, & F_3 &= 2\kappa_a\omega_2\omega, & F_4 &= -(\kappa_c + \omega_{\text{fb},1})\omega, \\
F_6 &= G_a g_{\text{cd},a}\omega_{\text{fb},a}E_1, & F_7 &= F_1 G_a g_{\text{cd},a}\omega_{\text{fb},a}, & F_8 &= -(E_4 + 2\kappa_a\omega_{\text{fb},a})\omega, & F_9 &= 2\kappa_a\omega^2 - E_4\omega_{\text{fb},a}, \\
E_2 &= \omega_2 G_2 g_{\text{cd},2}\omega_{\text{fb},2}F_8 + \omega_2 F_6, & E_3 &= \omega_2 G_2 g_{\text{cd},2}\omega_{\text{fb},2}F_9 + \omega_2 F_7, & E_4 &= \kappa_a^2 - \omega^2, & E_5 &= 2\kappa_a\omega, \\
E_6 &= (E_4\omega + E_5\gamma_2)A_1 - (E_4\gamma_2 - E_5\omega)B_1, & E_7 &= (E_4\omega + E_5\gamma_2)B_1 + (E_4\gamma_2 - E_5\omega)A_1, \\
E_8 &= \omega_2(F_2A_1 + F_3B_1) - \omega(E_6 + E_2), & E_9 &= \omega_2(F_2B_1 - F_3A_1) - \omega(E_7 + E_3), \\
E_{10} &= F_4E_8 - F_5E_9, & E_{11} &= F_4E_9 + F_5E_8, & E_{12} &= E_4\omega + 2\kappa_a\omega_{\text{fb},a}\omega, \\
E_{13} &= E_4\omega_{\text{fb},a} - 2\omega^2\kappa_a, & E_{14} &= E_{12}E_{10} + E_{13}E_{11}, & E_{15} &= E_{13}E_{10} - E_{12}E_{11}.
\end{aligned} \tag{A2}$$

-
- [1] T. J. Kippenberg and K. J. Vahala, Cavity optomechanics: Back-action at the mesoscale, *Science* **321**, 1172 (2008).
- [2] P. Meystre, A short walk through quantum optomechanics, *Ann. Phys. (Berlin)* **525**, 215 (2013).
- [3] M. Aspelmeyer, T. J. Kippenberg, and F. Marquardt, Cavity optomechanics, *Rev. Mod. Phys.* **86**, 1391 (2014).
- [4] S. Mancini, V. Giovannetti, D. Vitali, and P. Tombesi, Entangling Macroscopic Oscillators Exploiting Radiation Pressure, *Phys. Rev. Lett.* **88**, 120401 (2002).
- [5] L. Tian and P. Zoller, Coupled Ion-Nanomechanical Systems, *Phys. Rev. Lett.* **93**, 266403 (2004).
- [6] F. Massel, S. U. Cho, J.-M. Pirkkalainen, P. J. Hakonen, T. T. Heikkilä, and M. A. Sillanpää, Multimode circuit optomechanics near the quantum limit, *Nat. Commun.* **3**, 987 (2012).
- [7] A. Mari, A. Farace, N. Didier, V. Giovannetti, and R. Fazio, Measures of Quantum Synchronization in Continuous Variable Systems, *Phys. Rev. Lett.* **111**, 103605 (2013).
- [8] M. H. Matheny, M. Grau, L. G. Villanueva, R. B. Karabalin, M. C. Cross, and M. L. Roukes, Phase Synchronization of Two Anharmonic Nanomechanical Oscillators, *Phys. Rev. Lett.* **112**, 014101 (2014).
- [9] M. Zhang, S. Shah, J. Cardenas, and M. Lipson, Synchronization and Phase Noise Reduction in Micromechanical Oscillator Arrays Coupled Through Light, *Phys. Rev. Lett.* **115**, 163902 (2015).
- [10] C. F. Ockeloen-Korppi, E. Damskägg, J.-M. Pirkkalainen, M. Asjad, A. A. Clerk, F. Massel, M. J. Woolley, and M. A. Sillanpää, Stabilized entanglement of massive mechanical oscillators, *Nature (London)* **556**, 478 (2018).
- [11] R. Riedinger, A. Wallucks, I. Marinković, C. Lössnauer, M. Aspelmeyer, S. Hong, and S. Gröblacher, Remote quantum entanglement between two micromechanical oscillators, *Nature (London)* **556**, 473 (2018).
- [12] W. Qin, A. Miranowicz, G. L. Long, J. Q. You, and F. Nori, Proposal to test quantum wave-particle superposition on massive mechanical resonators, *npj Quantum Inf.* **5**, 58 (2019).
- [13] O. Di Stefano, A. Settineri, V. Macrì, A. Ridolfo, R. Stassi, A. F. Kockum, S. Savasta, and F. Nori, Interaction of Mechanical Oscillators Mediated by the Exchange of Virtual Photon Pairs, *Phys. Rev. Lett.* **122**, 030402 (2019).
- [14] S. Kotler *et al.*, Direct observation of deterministic macroscopic entanglement, *Science* **372**, 622 (2021).
- [15] L. Mercier de Lépinay, C. F. Ockeloen-Korppi, M. J. Woolley, and M. A. Sillanpää, Quantum mechanics-free subsystem with mechanical oscillators, *Science* **372**, 625 (2021).

- [16] H. Xu, D. Mason, L. Jiang, and J. G. E. Harris, Topological energy transfer in an optomechanical system with exceptional points, *Nature (London)* **537**, 80 (2016).
- [17] G. Heinrich, M. Ludwig, J. Qian, B. Kubala, and F. Marquardt, Collective Dynamics in Optomechanical Arrays, *Phys. Rev. Lett.* **107**, 043603 (2011).
- [18] A. Xuereb, C. Genes, and A. Dantan, Strong Coupling and Long-Range Collective Interactions in Optomechanical Arrays, *Phys. Rev. Lett.* **109**, 223601 (2012).
- [19] M. Ludwig and F. Marquardt, Quantum Many-Body Dynamics in Optomechanical Arrays, *Phys. Rev. Lett.* **111**, 073603 (2013).
- [20] A. Xuereb, C. Genes, G. Pupillo, M. Paternostro, and A. Dantan, Reconfigurable Long-Range Phonon Dynamics in Optomechanical Arrays, *Phys. Rev. Lett.* **112**, 133604 (2014).
- [21] A. Xuereb, A. Imparato, and A. Dantan, Heat transport in harmonic oscillator systems with thermal baths: Application to optomechanical arrays, *New J. Phys.* **17**, 055013 (2015).
- [22] O. Černotík, S. Mahmoodian, and K. Hammerer, Spatially Adiabatic Frequency Conversion in Optoelectromechanical Arrays, *Phys. Rev. Lett.* **121**, 110506 (2018).
- [23] P. Rabl, S. J. Kolkowitz, F. H. L. Koppens, J. G. E. Harris, P. Zoller, and M. D. Lukin, A quantum spin transducer based on nanoelectromechanical resonator arrays, *Nat. Phys.* **6**, 602 (2010).
- [24] D.-G. Lai, X. Wang, W. Qin, B.-P. Hou, F. Nori, and J.-Q. Liao, Tunable optomechanically induced transparency by controlling the dark-mode effect, *Phys. Rev. A* **102**, 023707 (2020).
- [25] S. C. Masmanidis, R. B. Karabalin, I. D. Vlamincik, G. Borghs, M. R. Freeman, and M. L. Roukes, Multifunctional nanomechanical systems via tunably coupled piezoelectric actuation, *Science* **317**, 780 (2007).
- [26] I. Mahboob and H. Yamaguchi, Bit storage and bit flip operations in an electromechanical oscillator, *Nat. Nanotechnol.* **3**, 275 (2008).
- [27] F. Massel, T. T. Heikkilä, J.-M. Pirkkalainen, S. U. Cho, H. Saloniemi, P. J. Hakonen, and M. A. Sillanpää, Microwave amplification with nanomechanical resonators, *Nature (London)* **480**, 351 (2011).
- [28] P. Huang, P. Wang, J. Zhou, Z. Wang, C. Ju, Z. Wang, Y. Shen, C. Duan, and J. Du, Demonstration of Motion Transduction Based on Parametrically Coupled Mechanical Resonators, *Phys. Rev. Lett.* **110**, 227202 (2013).
- [29] P. Huang, L. Zhang, J. Zhou, T. Tian, P. Yin, C. Duan, and J. Du, Nonreciprocal Radio Frequency Transduction in a Parametric Mechanical Artificial Lattice, *Phys. Rev. Lett.* **117**, 017701 (2016).
- [30] D. Malz, L. D. Tóth, N. R. Bernier, A. K. Feofanov, T. J. Kippenberg, and A. Nunnenkamp, Quantum-Limited Directional Amplifiers with Optomechanics, *Phys. Rev. Lett.* **120**, 023601 (2018).
- [31] Z. Shen, Y.-L. Zhang, Y. Chen, C.-L. Zou, Y.-F. Xiao, X.-B. Zou, F.-W. Sun, G.-C. Guo, and C.-H. Dong, Experimental realization of optomechanically induced non-reciprocity, *Nat. Photon.* **10**, 657 (2016).
- [32] Z. Shen, Y.-L. Zhang, Y. Chen, F.-W. Sun, X.-B. Zou, G.-C. Guo, C.-L. Zou, and C.-H. Dong, Reconfigurable optomechanical circulator and directional amplifier, *Nat. Commun.* **9**, 1797 (2018).
- [33] K. Fang, J. Luo, A. Metelmann, M. H. Matheny, F. Marquardt, A. A. Clerk, and O. Painter, Generalized non-reciprocity in an optomechanical circuit via synthetic magnetism and reservoir engineering, *Nat. Phys.* **13**, 465 (2017).
- [34] H. Xu, L. Jiang, A. A. Clerk, and J. G. E. Harris, Nonreciprocal control and cooling of phonon modes in an optomechanical system, *Nature (London)* **568**, 65 (2019).
- [35] J. P. Mathew, J. D. Pino, and E. Verhagen, Synthetic gauge fields for phonon transport in a nano-optomechanical system, *Nat. Nanotechnol.* **15**, 198 (2020).
- [36] C. Yang, X. Wei, J. Sheng, and H. Wu, Phonon heat transport in cavity-mediated optomechanical nanoresonators, *Nat. Commun.* **11**, 4656 (2020).
- [37] C. Sanavio, V. Peano, and A. Xuereb, Nonreciprocal topological phononics in optomechanical arrays, *Phys. Rev. B* **101**, 085108 (2020).
- [38] I. Wilson-Rae, N. Nooshi, W. Zwerger, and T. J. Kippenberg, Theory of Ground State Cooling of a Mechanical Oscillator Using Dynamical Backaction, *Phys. Rev. Lett.* **99**, 093901 (2007).
- [39] F. Marquardt, J. P. Chen, A. A. Clerk, and S. M. Girvin, Quantum Theory of Cavity-Assisted Sideband Cooling of Mechanical Motion, *Phys. Rev. Lett.* **99**, 093902 (2007).
- [40] C. Genes, D. Vitali, P. Tombesi, S. Gigan, and M. Aspelmeyer, Ground-state cooling of a micromechanical oscillator: Comparing cold damping and cavity-assisted cooling schemes, *Phys. Rev. A* **77**, 033804 (2008).
- [41] S. Mancini, D. Vitali, and P. Tombesi, Optomechanical Cooling of a Macroscopic Oscillator by Homodyne Feedback, *Phys. Rev. Lett.* **80**, 688 (1998).
- [42] P. F. Cohadon, A. Heidmann, and M. Pinard, Cooling of a Mirror by Radiation Pressure, *Phys. Rev. Lett.* **83**, 3174 (1999).
- [43] V. Steixner, P. Rabl, and P. Zoller, Quantum feedback cooling of a single trapped ion in front of a mirror, *Phys. Rev. A* **72**, 043826 (2005).
- [44] P. Bushev, D. Rotter, A. Wilson, F. M. C. Dubin, C. Becher, J. Eschner, R. Blatt, V. Steixner, P. Rabl, and P. Zoller, Feedback Cooling of a Single Trapped Ion, *Phys. Rev. Lett.* **96**, 043003 (2006).
- [45] M. Rossi, N. Kralj, S. Zippilli, R. Natali, A. Borrielli, G. Pandraud, E. Serra, G. D. Giuseppe, and D. Vitali, Enhancing Sideband Cooling by Feedback-Controlled Light, *Phys. Rev. Lett.* **119**, 123603 (2017).
- [46] M. Rossi, D. Mason, J. Chen, Y. Tsaturyan, and A. Schliesser, Measurement-based quantum control of mechanical motion, *Nature (London)* **563**, 53 (2018).
- [47] G. P. Conangla, F. Ricci, M. T. Cuairan, A. W. Schell, N. Meyer, and R. Quidant, Optimal Feedback Cooling of a Charged Levitated Nanoparticle with Adaptive Control, *Phys. Rev. Lett.* **122**, 223602 (2019).
- [48] F. Tebbenjohanns, M. Frimmer, A. Militaru, V. Jain, and L. Novotny, Cold Damping of an Optically Levitated Nanoparticle to Microkelvin Temperatures, *Phys. Rev. Lett.* **122**, 223601 (2019).
- [49] C. Sommer and C. Genes, Partial Optomechanical Refrigeration Via Multimode Cold-Damping Feedback, *Phys. Rev. Lett.* **123**, 203605 (2019).
- [50] J. Guo, R. Norte, and S. Gröblacher, Feedback Cooling of a Room Temperature Mechanical Oscillator Close to Its Motional Ground State, *Phys. Rev. Lett.* **123**, 223602 (2019).

- [51] C. Sommer, A. Ghosh, and C. Genes, Multimode cold-damping optomechanics with delayed feedback, *Phys. Rev. Research* **2**, 033299 (2020).
- [52] F. Tebbenjohanns, M. Frimmer, V. Jain, D. Windey, and L. Novotny, Motional Sideband Asymmetry of a Nanoparticle Optically Levitated in Free Space, *Phys. Rev. Lett.* **124**, 013603 (2020).
- [53] L. Magrini, P. Rosenzweig, C. Bach, A. Deutschmann-Olek, S. G. Hofer, S. Hong, N. Kiesel, A. Kugi, and M. Aspelmeyer, Real-time optimal quantum control of mechanical motion at room temperature, *Nature (London)* **595**, 373 (2021).
- [54] F. Tebbenjohanns, M. L. Mattana, M. Rossi, M. Frimmer, and L. Novotny, Quantum control of a nanoparticle optically levitated in cryogenic free space, *Nature (London)* **595**, 378 (2021).
- [55] Y.-C. Liu, Y.-F. Xiao, X. Luan, and C. W. Wong, Dynamic Dissipative Cooling of a Mechanical Resonator in Strong Coupling Optomechanics, *Phys. Rev. Lett.* **110**, 153606 (2013).
- [56] Y.-C. Liu, Y.-F. Shen, Q. Gong, and Y.-F. Xiao, Optimal limits of cavity optomechanical cooling in the strong-coupling regime, *Phys. Rev. A* **89**, 053821 (2014).
- [57] X.-T. Wang, S. Vinjanampathy, F. W. Strauch, and K. Jacobs, Ultraefficient Cooling of Resonators: Beating Sideband Cooling with Quantum Control, *Phys. Rev. Lett.* **107**, 177204 (2011).
- [58] Y. Li, L.-A. Wu, Y.-D. Wang, and L.-P. Yang, Nondeterministic ultrafast ground-state cooling of a mechanical resonator, *Phys. Rev. B* **84**, 094502 (2011).
- [59] L.-L. Yan, J.-Q. Zhang, S. Zhang, and M. Feng, Efficient cooling of quantized vibrations using a four-level configuration, *Phys. Rev. A* **94**, 063419 (2016).
- [60] J.-Q. Liao and C. K. Law, Cooling of a mirror in cavity optomechanics with a chirped pulse, *Phys. Rev. A* **84**, 053838 (2011).
- [61] S. Machnes, J. Cerrillo, M. Aspelmeyer, W. Wieczorek, M. B. Plenio, and A. Retzker, Pulsed Laser Cooling for Cavity Optomechanical Resonators, *Phys. Rev. Lett.* **108**, 153601 (2012).
- [62] D.-G. Lai, J.-F. Huang, X.-L. Yin, B.-P. Hou, W. Li, D. Vitali, F. Nori, and J.-Q. Liao, Nonreciprocal ground-state cooling of multiple mechanical resonators, *Phys. Rev. A* **102**, 011502(R) (2020).
- [63] D.-G. Lai, F. Zou, B.-P. Hou, Y.-F. Xiao, and J.-Q. Liao, Simultaneous cooling of coupled mechanical resonators in cavity optomechanics, *Phys. Rev. A* **98**, 023860 (2018).
- [64] D.-G. Lai, J. Huang, B.-P. Hou, F. Nori, and J.-Q. Liao, Domino cooling of a coupled mechanical-resonator chain via cold-damping feedback, *Phys. Rev. A* **103**, 063509 (2021).
- [65] J. Chan, T. P. Alegre, A. H. Safavi-Naeini, J. T. Hill, A. Krause, S. Groblacher, M. Aspelmeyer, and O. Painter, Laser cooling of a nanomechanical oscillator into its quantum ground state, *Nature (London)* **478**, 89 (2011).
- [66] J. D. Teufel, T. Donner, D. Li, J. W. Harlow, M. S. Allman, K. Cicak, A. J. Sirois, J. D. Whittaker, K. W. Lehnert, and R. W. Simmonds, Sideband cooling of micromechanical motion to the quantum ground state, *Nature (London)* **475**, 359 (2011).
- [67] J. B. Clark, F. Lecocq, R. W. Simmonds, J. Aumentado, and J. D. Teufel, Sideband cooling beyond the quantum backaction limit with squeezed light, *Nature (London)* **541**, 191 (2017).
- [68] M. Xu, X. Han, C.-L. Zou, W. Fu, Y. Xu, C. Zhong, L. Jiang, and H. X. Tang, Radiative Cooling of a Superconducting Resonator, *Phys. Rev. Lett.* **124**, 033602 (2020).
- [69] L. Qiu, I. Shomroni, P. Seidler, and T. J. Kippenberg, Laser Cooling of a Nanomechanical Oscillator to Its Zero-Point Energy, *Phys. Rev. Lett.* **124**, 173601 (2020).
- [70] F. Xue, Y. D. Wang, Y. X. Liu, and F. Nori, Cooling a micro-mechanical beam by coupling it to a transmission line, *Phys. Rev. B* **76**, 205302 (2007).
- [71] J. Q. You, Y. X. Liu, and F. Nori, Simultaneous Cooling of an Artificial Atom and Its Neighboring Quantum System, *Phys. Rev. Lett.* **100**, 047001 (2008).
- [72] J. Zhang, Y. X. Liu, and F. Nori, Cooling and squeezing the fluctuations of a nanomechanical beam by indirect quantum feedback control, *Phys. Rev. A* **79**, 052102 (2009).
- [73] S. De Liberato, N. Lambert, and F. Nori, Quantum noise in photothermal cooling, *Phys. Rev. A* **83**, 033809 (2011).
- [74] M. Grajcar, S. Ashhab, J. R. Johansson, and F. Nori, Lower limit on the achievable temperature in resonator-based sideband cooling, *Phys. Rev. B* **78**, 035406 (2008).
- [75] F. Nori, Atomic physics with a circuit, *Nat. Phys.* **4**, 589 (2008).
- [76] Z. L. Xiang, S. Ashhab, J. Q. You, and F. Nori, Hybrid quantum circuits: Superconducting circuits interacting with other quantum systems, *Rev. Mod. Phys.* **85**, 623 (2013).
- [77] M. O. Scully and M. S. Zubairy, *Quantum Optics* (Cambridge University Press, Cambridge, UK, 1997).
- [78] G. S. Agarwal, *Quantum Optics* (Cambridge University Press, Cambridge, UK, 2013).
- [79] C. Genes, D. Vitali, and P. Tombesi, Simultaneous cooling and entanglement of mechanical modes of a micromirror in an optical cavity, *New J. Phys.* **10**, 095009 (2008).
- [80] A. B. Shkarin, N. E. Flowers-Jacobs, S. W. Hoch, A. D. Kashkanova, C. Deutsch, J. Reichel, and J. G. E. Harris, Optically Mediated Hybridization Between Two Mechanical Modes, *Phys. Rev. Lett.* **112**, 013602 (2014).
- [81] M. C. Kuzyk and H. Wang, Controlling multimode optomechanical interactions via interference, *Phys. Rev. A* **96**, 023860 (2017).
- [82] C. F. Ockeloen-Korppi, M. F. Gely, E. Damskäg, M. Jenkins, G. A. Steele, and M. A. Sillanpää, Sideband cooling of nearly degenerate micromechanical oscillators in a multimode optomechanical system, *Phys. Rev. A* **99**, 023826 (2019).
- [83] J. Huang, D.-G. Lai, C. Liu, J.-F. Huang, F. Nori, and J.-Q. Liao, Multimode optomechanical cooling via general dark-mode control, *Phys. Rev. A* **106**, 013526 (2022).
- [84] J.-Y. Liu, W. Liu, D. Xu, J.-C. Shi, H. Xu, Q. Gong, and Y.-F. Xiao, Ground-state cooling of multiple near-degenerate mechanical modes, *Phys. Rev. A* **105**, 053518 (2022).
- [85] K. Jacobs, *Quantum Measurement Theory and its Application* (Cambridge University Press, Cambridge, UK, 2014).
- [86] D.-G. Lai, W. Qin, B.-P. Hou, A. Miranowicz, and F. Nori, Significant enhancement in refrigeration and entanglement in auxiliary-cavity-assisted optomechanical systems, *Phys. Rev. A* **104**, 043521 (2021).
- [87] N. R. Bernier, L. D. Tóth, A. Koottandavida, M. A. Ioannou, D. Malz, A. Nunnenkamp, A. K. Feofanov, and T. J. Kippenberg, Nonreciprocal reconfigurable microwave optomechanical circuit, *Nat. Commun.* **8**, 604 (2017).
- [88] G. A. Peterson, F. Lecocq, K. Cicak, R. W. Simmonds, J. Aumentado, and J. D. Teufel, Demonstration of Efficient Nonreciprocity in a Microwave Optomechanical Circuit, *Phys. Rev. X* **7**, 031001 (2017).